NeuroResource

Neuron

Plug-and-Play Protein Modification Using Homology-Independent Universal Genome Engineering

Graphical Abstract

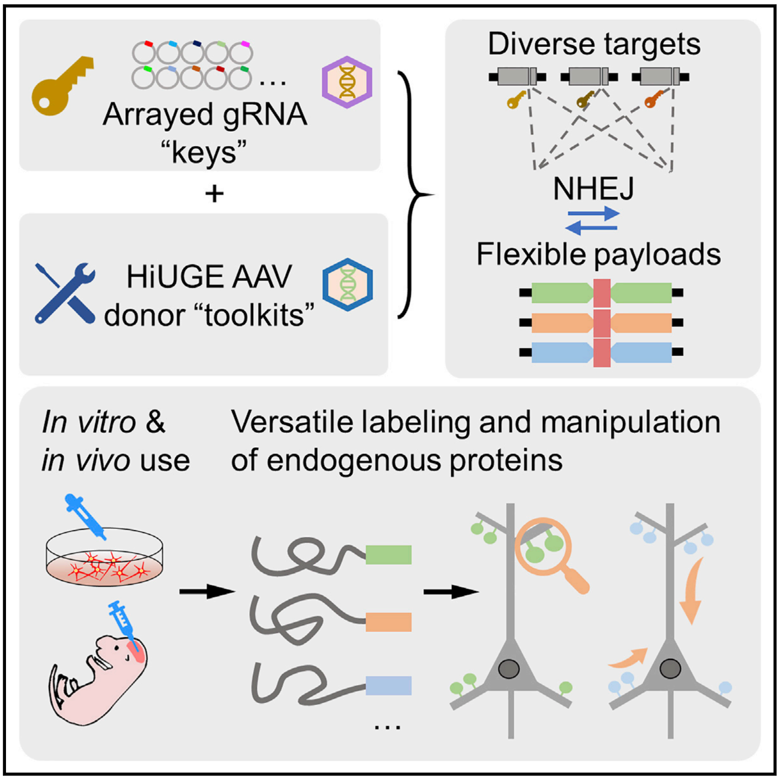
Arrayed gRNA
"keys"
+
HiUGE AAV
donor "toolkits"
Diverse targets
NHEJ
Flexible payloads
In vitro &
in vivo use
Versatile labeling and manipulation
of endogenous proteins
...

Highlights

- HiUGE, an AAV-based CRISPR-mediated method for universal insertional genome editing
- Arrayed gRNAs and premade donors enable high-throughput endogenous protein labeling
- "Plug-and-play" selection of donors at each target locus enables diverse applications
- HiUGE provides a powerful method to analyze proteomic candidates *in vitro* and *in vivo*

Authors

Yudong Gao, Erin Hisey,
Tyler W.A. Bradshaw, ..., Yu Xiang,
Yarui Diao, Scott H. Soderling

Correspondence

scott.soderling@duke.edu

In Brief

Gao et al. developed an AAV-based CRISPR-mediated homology-independent universal genome engineering (HiUGE) method for high-throughput modification of endogenous proteins, enabling scalable, flexible, and diverse applications such as localization mapping and functional interrogation of proteins *in vitro* and *in vivo*.

Gao et al., 2019, Neuron *103*, 1–15
August 21, 2019 © 2019 Elsevier Inc.
https://doi.org/10.1016/j.neuron.2019.05.047

CellPress

Please cite this article in press as: Gao et al., Plug-and-Play Protein Modification Using Homology-Independent Universal Genome Engineering, Neuron (2019), https://doi.org/10.1016/j.neuron.2019.05.047

Neuron
NeuroResource

Plug-and-Play Protein Modification Using Homology-Independent Universal Genome Engineering

Yudong Gao,[1] Erin Hisey,[1] Tyler W.A. Bradshaw,[1,2] Eda Erata,[1] Walter E. Brown,[1] Jamie L. Courtland,[1,2] Akiyoshi Uezu,[1] Yu Xiang,[1] Yarui Diao,[1] and Scott H. Soderling[1,2,3,*]
[1]Department of Cell Biology, Duke University Medical School, Durham, NC 27710, USA
[2]Department of Neurobiology, Duke University Medical School, Durham, NC 27710, USA
[3]Lead Contact
*Correspondence: scott.soderling@duke.edu
https://doi.org/10.1016/j.neuron.2019.05.047

SUMMARY

Analysis of endogenous protein localization, function, and dynamics is fundamental to the study of all cells, including the diversity of cell types in the brain. However, current approaches are often low throughput and resource intensive. Here, we describe a CRISPR-Cas9-based homology-independent universal genome engineering (HiUGE) method for endogenous protein manipulation that is straightforward, scalable, and highly flexible in terms of genomic target and application. HiUGE employs adeno-associated virus (AAV) vectors of autonomous insertional sequences (payloads) encoding diverse functional modifications that can integrate into virtually any genomic target loci specified by easily assembled gene-specific guide-RNA (GS-gRNA) vectors. We demonstrate that universal HiUGE donors enable rapid alterations of proteins *in vitro* or *in vivo* for protein labeling and dynamic visualization, neural-circuit-specific protein modification, subcellular rerouting and sequestration, and truncation-based structure-function analysis. Thus, the "plug-and-play" nature of HiUGE enables high-throughput and modular analysis of mechanisms driving protein functions in cellular neurobiology.

INTRODUCTION

Selective labeling and manipulation of endogenous proteins are essential to delineating the molecular mechanisms of cell and organismal biology. Recent advances in exploratory proteomics and gene expression analysis generate sizable datasets that urgently require high-throughput and reliable methods for protein visualization and functional manipulation purposes. However, current techniques to enable these strategies are often inefficient or resource intensive. For example, due to the limited availability and the cost of antibodies, it is often not a viable option for single labs to immunolabel tens to hundreds of proteomic candidates. Further, a large fraction of available antibodies may have limited utility due to unsuspected cross-reactivity to other proteins, lot-to-lot variability in quality, and insufficient application-specific validation (Berglund et al., 2008; Bradbury and Plückthun, 2015; Egelhofer et al., 2011; Michel et al., 2009). Additionally, overexpression of recombinant constructs to map protein localization or conduct functional analyses is also resource intensive and can be highly sensitive to available cellular docking sites or unforeseen artifactual cellular effects associated with protein overexpression.

CRISPR-associated endonuclease Cas9-based strategies have great promise to enable highly precise genome editing of mammalian cells to address many of the above limitations (Cong et al., 2013; Doudna and Charpentier, 2014; Hsu et al., 2014; Jinek et al., 2012; Mali et al., 2013). CRISPR-Cas9 introduces double-strand breaks (DSBs) at guide RNA (gRNA) specified genomic sites. These genomic DSBs are repaired via two main pathways in cells; non-homologous end joining (NHEJ) is the prevailing pathway, while homology-directed repair (HDR) is reportedly less frequent, especially in non-dividing cells outside of the S and G2 phase of cell cycle (Heyer et al., 2010; Hsu et al., 2014; Mao et al., 2008; Saleh-Gohari and Helleday, 2004). Both HDR and NHEJ pathways are currently utilized to insert foreign DNA sequences into genes of interest (GOIs) for applications such as labeling of translated endogenous protein products.

Examples of these methods include single-cell labeling of endogenous proteins (SLENDR and viral SLENDR [(v)SLENDR]) and homology-independent targeted integration (HITI), both of which have been shown to function in post-mitotic cells, including neurons. SLENDR is based on HDR, using oligonucleotides or adeno-associated virus (AAV) donors containing gene-specific homology sequences to facilitate insertion into GOIs (Mikuni et al., 2016; Nishiyama et al., 2017). Alternatively, HITI leverages NHEJ to insert foreign sequences into a GOI. It utilizes donor vectors containing gene-specific gRNA recognition sequences, which simultaneously direct DSB cuts to the gene and donor vector, facilitating directional insertion during NHEJ (Suzuki et al., 2016). Although SLENDR and HITI are flexible in their ability to modify proteins both *in vitro* and *in vivo* for neuronal applications, they both necessitate the cloning of gRNA vectors for the GOIs, as well as customized gene-specific donor vectors for each insertion. By requiring the generation of tailored donor vectors for each DSB cut site in each GOI, the scalability and throughput of testing multiple insertional sequences using either SLENDR or HITI are limited. Alternatively, CRISPaint pairs NHEJ with modular donor vectors that are linearized and integrated into GOIs and demonstrates improved throughput for insertional editing in cell lines (Schmid-Burgk et al., 2016). However, it requires specially prepared mini-circular vectors that are not compatible with viral delivery methods important for many *in vivo* applications, or the bacterial vector backbones are necessarily co-inserted into genomes, which can interfere long-term transgene expression (Chen et al., 2001b, 2003). These issues may limit its widespread utility, especially for applications where viral transduction is preferred *in vitro* or *in vivo*.

Here, we describe homology-independent universal genome engineering (HiUGE), a new generalized method that obviates many of the constraints to the current state of the art. HiUGE is an AAV-mediated method that uses a two-vector modular approach for higher-throughput genomic knockin (KI) applications. The donor vector contains an insertional DNA fragment (payload) that is flanked on both ends by an artificial DNA sequence non-homologous to the target genome. This sequence is recognized by a donor-specific gRNA (DS-gRNA) that directs the Cas9-mediated autonomous excision and release of the payload. The payload can then be integrated across diverse GOIs, both *in vitro* and *in vivo*, at genomic loci specified by a separate panel of high-throughput and low-cost gene-specific gRNA (GS-gRNA) vectors. This design frees the donor vectors of any gene-specific sequences, rendering them universally compatible for virtually any CRISPR-Cas9-accessible genomic loci. Importantly, these AAV donors can be premade for ubiquitous applications, greatly simplifying strategies for insertional genome editing. We have tested payloads for a variety of applications and demonstrate their interchangeability within and between GOIs in both cells and tissues. These applications include antibody epitope and fluorescent protein labeling for localization mapping and dynamic visualization of endogenous proteins, protein subcellular rerouting and sequestration, protein truncation for structure-function relationship analysis, and neural-circuit-specific genome engineering. Because this method is highly modular, scalable, and suitable for *in vitro* as well as *in vivo* applications, it opens new avenues to pair higher-throughput proteomic and genomic applications with experimental validation and phenotypic screening to address molecular mechanisms of cellular neurobiology.

RESULTS

HiUGE Concept and Its Specificity to Modify Endogenous Proteins

Recent advances in proteomics and gene expression studies generate sizable protein and gene network datasets, which urgently require novel methods to analyze them on larger scales with greater precision. Higher-throughput genome engineering techniques targeting candidate proteins/genes could satisfy these needs. We thus designed a method utilizing the delivery of universal DNA inserts (payloads) that can ubiquitously integrate across genes to achieve this. In the HiUGE system (Figure 1A), a two-vector approach was used to deliver GS-gRNAs and universal payloads, with AAV as the delivery vehicle for its flexible use *in vitro* and *in vivo*. HiUGE GS-gRNA vectors are prepared by ligations of 23- to 24-mer oligonucleotides to the backbone vector, which is scalable to generate panels of gRNA expressing vectors targeting diverse GOIs. HiUGE donor vectors are autonomous, expressing a synthetic donor-specific gRNA (DS-gRNA) that is non-homologous to the targeted genome but directs Cas9-mediated self-cleavage and release of the universal payloads for genomic insertion. This design allows the separation of the donor vector construction from any specific sequence of genomic targets, thus enabling universal applications of the donor "toolkits." Such utilities include localization mapping and functional manipulation of the endogenous proteins, by introducing tags at their carboxy- or amino-terminus (C- or N-term) within diverse CRISPR-Cas9-accessible genomic loci unlocked by the GS-gRNA "keys."

To test this concept, a dual-orientation payload design was used to facilitate the expression of a hemagglutinin (HA)-epitope tag following either forward or reverse integration into the C-term of proteins of interest (Figure 1B). We adopted a protocol to produce small-scale transduction-ready AAVs for higher-throughput use *in vitro*, complimenting traditional AAV purifications for use *in vivo* (Figure 1C; STAR Methods). As a proof of concept, small-scale AAVs of a GS-gRNA targeting the mouse *Tubb3* gene and a dual-orientation HA-epitope HiUGE donor were used to co-transduce primary neurons prepared from neonatal pups of conditional Cas9 mice. The GS-gRNA AAV also expresses Cre-recombinase to induce Cas9-2A-GFP expression. Approximately 1 week following infection, immunofluorescent detection of HA-epitope showed successful labeling of endogenous βIII-tubulin, with localization characteristics specific to microtubules (Figures 1D and S1A). Western blot detection of the HA-epitope showed a single band (~51 kDa) consistent with the predicted molecular mass of βIII-tubulin (Figure 1E). Genomic insertion of the payload was verified by sequencing the *Tubb3* locus, confirming the successful HA-epitope integration (Figure 1F). In control experiments, the relative selectivity of frame-dependent labeling was tested by comparing the correct open reading frame (ORF) donor (ORF+1, in reference to the Cas9 cleavage locus specified by the *Tubb3* gRNA) to out-of-frame donors (ORF+0 or ORF+2) (Figure S1B i–iii). HA-labeling in the correct ORF was substantially more efficient (Figure S1C), with occasional HA-positive cells observed from out-of-frame ORFs, indicating comparatively less frequent frameshifting insertion or deletion (indel) events during payload integration. Negative controls demonstrated the absolute requirement for both GS-gRNA and HiUGE donor vectors for HA-epitope KI (Figure S1B iv–vi). To demonstrate that donor vectors for all three ORFs are equally capable of facilitating HiUGE, three GS-gRNAs, one for each ORF, were designed to target the mouse *Map2* gene. Pairing these GS-gRNA AAVs with HA-epitope donor AAVs in their corresponding ORFs resulted in comparable and efficient labeling (Figures S1D and S1E).

An important consideration is that the HiUGE donor vectors should be suitable to target diverse coding sequences without introducing premature stop codons that prevent proper expression of the insert. This is achieved by using donor recognition sequences (DRSs) specifically designed such that premature stop codons cannot be introduced during genomic integration. We compared HA-epitope donor vectors with different DRSs and found similar cellular labeling efficiencies among them (Figures

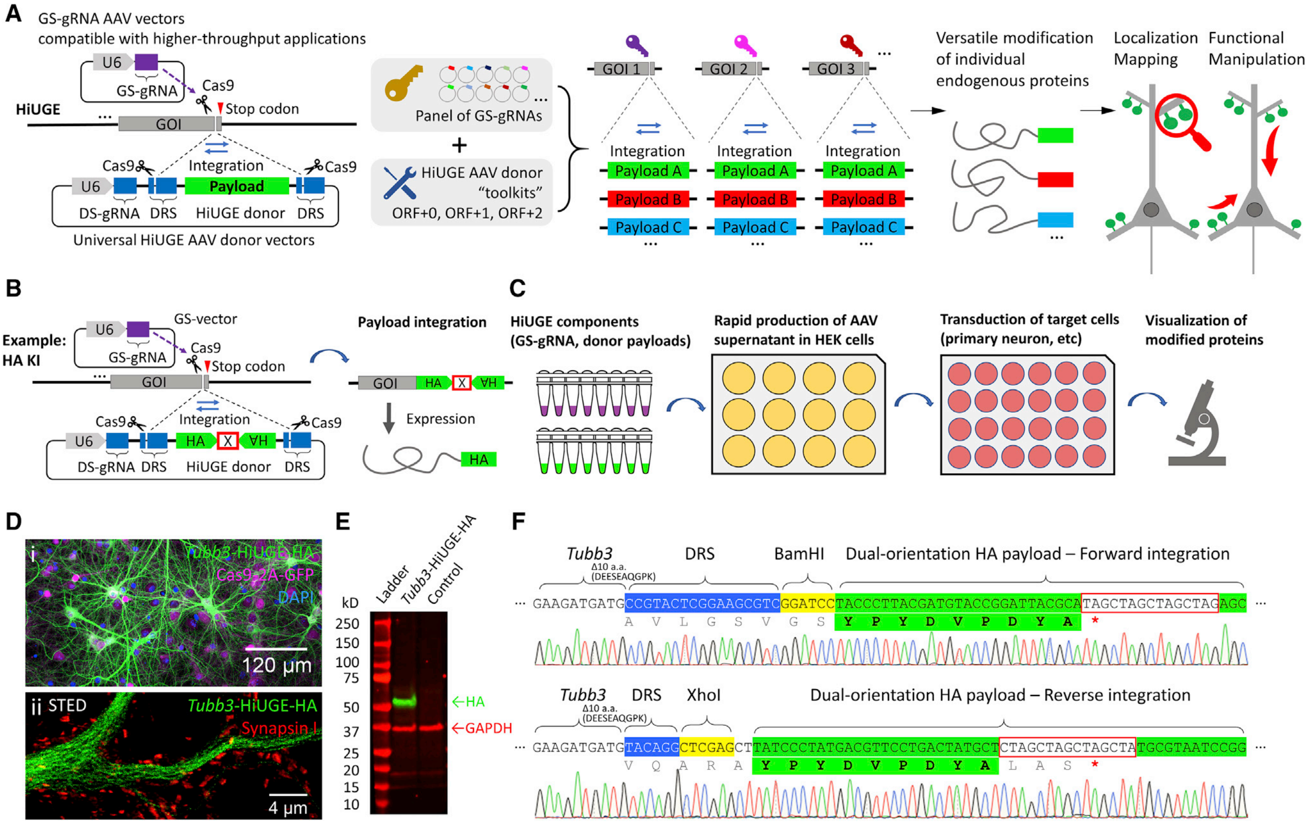
A
GS-gRNA AAV vectors
compatible with higher-throughput applications
U6
GS-gRNA
Cas9
Stop codon
HiUGE
GOI
Cas9
Integration
Cas9
U6
Payload
DS-gRNA
DRS
HiUGE donor
DRS
Universal HiUGE AAV donor vectors
Panel of GS-gRNAs
+
HiUGE AAV donor "toolkits"
ORF+0, ORF+1, ORF+2
GOI 1
GOI 2
GOI 3
Integration
Payload A
Payload B
Payload C
Versatile modification of individual endogenous proteins
Localization Mapping
Functional Manipulation
B
Example: HA KI
GS-vector
Payload integration
HA
X
Expression
C
HiUGE components (GS-gRNA, donor payloads)
Rapid production of AAV supernatant in HEK cells
Transduction of target cells (primary neuron, etc)
Visualization of modified proteins
D
i
Tubb3-HiUGE-HA
Cas9-2A-GFP
DAPI
120 μm
ii STED
Tubb3-HiUGE-HA
Synapsin I
4 μm
E
Ladder
Tubb3-HiUGE-HA
Control
kD
250
150
100
75
50
37
25
20
15
10
←HA
←GAPDH
F
Tubb3
Δ10 a.a. (DEESEAQGPK)
DRS
BamHI
Dual-orientation HA payload – Forward integration
··· GAAGATGATGCCGTACTCGGAAGCGTCGGATCCTACCCTTACGATGTACCGGATTACGCATAGCTAGCTAGCTAGAGC ···
A V L G S V G S Y P Y D V P D Y A *
Tubb3
Δ10 a.a. (DEESEAQGPK)
DRS
XhoI
Dual-orientation HA payload – Reverse integration
··· GAAGATGATGTACAGGCTCGAGCTTATCCCTATGACGTTCCTGACTATGCTCTAGCTAGCTAGCTATGCGTAATCCGG ···
V Q A R A Y P Y D V P D Y A L A S *

Figure 1. Illustration of the HiUGE System

(A) Schematic of HiUGE method. The HiUGE donor vector expresses a donor-specific gRNA (DS-gRNA), which specifically recognizes the donor recognition sequence (DRS) and directs the cleavage and release of the donor payload for insertion into gene-specific gRNA (GS-gRNA) targeted loci for modification of proteins.

(B) HiUGE donor vectors harboring short epitope tags employ a dual-orientation design for efficient expression following either forward or reverse genomic integration. A cassette of stop codons for all six ORFs (denoted by an "X" boxed in red, sequence listed in Table S1) is used to terminate translation.

(C) Workflow using a small-scale, low-cost, and higher-throughput AAV supernatant production method for *in vitro* applications.

(D–F) Proof-of-principle data showing HA-epitope KI to mouse *Tubb3* gene in primary neuron culture of Cas9 mice after transduction with a combination of small-scale GS-gRNA AAV and HA-epitope donor AAV.

(D) Representative (i) confocal and (ii) stimulated emission depletion (STED) images of immunocytochemistry staining for HA-epitope, showing the characteristic microtubule expression pattern of the HA-epitope-labeled ßIII-tubulin. GFP fluorescence of the Cas9-2A-GFP, nuclei labeling with DAPI, and synaptic marker synapsin I staining are also shown.

(E) Western blot for HA-epitope in a comparison against a negative control (transduced with empty GS-gRNA backbone and HiUGE donor), showing a single band of labeled protein at the expected molecular mass (~51 kDa) for ßIII-tubulin.

(F) Representative sequencing results showing correct integration in forward and reverse orientation. Regions of DNA sequence containing genomic *Tubb3*, DRS (blue shade), restriction enzymes (yellow shade), HA-epitope (green shade), and stop codon cassette (red box) are indicated. Truncated terminal amino acids are noted. Translated amino acid sequences encoded by the payload and the in-frame stop codon (red asterisk) are indicated as well.

S2A–S2C), demonstrating flexibility in DRS usage. Also, we found that the cellular labeling efficiency for HiUGE was comparable to HITI (Figures S2D–S2I).

Higher-Throughput Modification of Diverse Protein Targets by Universal HiUGE Payloads

We next tested whether a single HiUGE payload can be integrated across diverse genomic loci and label multiple target proteins for subcellular localization mapping. We used oligonucleotide ligation to rapidly construct an arrayed panel of GS-gRNA AAV vectors targeting the C terminus of 12 proteins, which exhibit previously described and highly patterned subcellular localizations in neurons and glia. These included proteins of the microtubule network (βIII-tubulin, *Tubb3*; microtubule-associated protein 2, *Map2*), the nucleus (methyl-CpG-binding protein 2, *Mecp2*; Chen et al., 2001a), the synaptic actin cytoskeleton (actin-related protein 2, *Actr2*; Kim et al., 2013; Spence and Soderling, 2015), clathrin-coated vesicles (clathrin light chain A, *Clta*), the axonal initial segment (AIS) (neuronal adhesion molecule, *Nrcam*; Ankyrin-G, *Ank3*; βIV-spectrin, *Sptbn4*; sodium channel subunit Nav1.2, *Scn2a*; Jones and Svitkina, 2016), intermediate filaments (glial fibrillary acidic protein, *Gfap*), mitochondria (pyruvate dehydrogenase E1 component subunit alpha, *Pdha1*), and the distal tips of neurites (Doublecortin, *Dcx*; Francis

Please cite this article in press as: Gao et al., Plug-and-Play Protein Modification Using Homology-Independent Universal Genome Engineering, Neuron (2019), https://doi.org/10.1016/j.neuron.2019.05.047

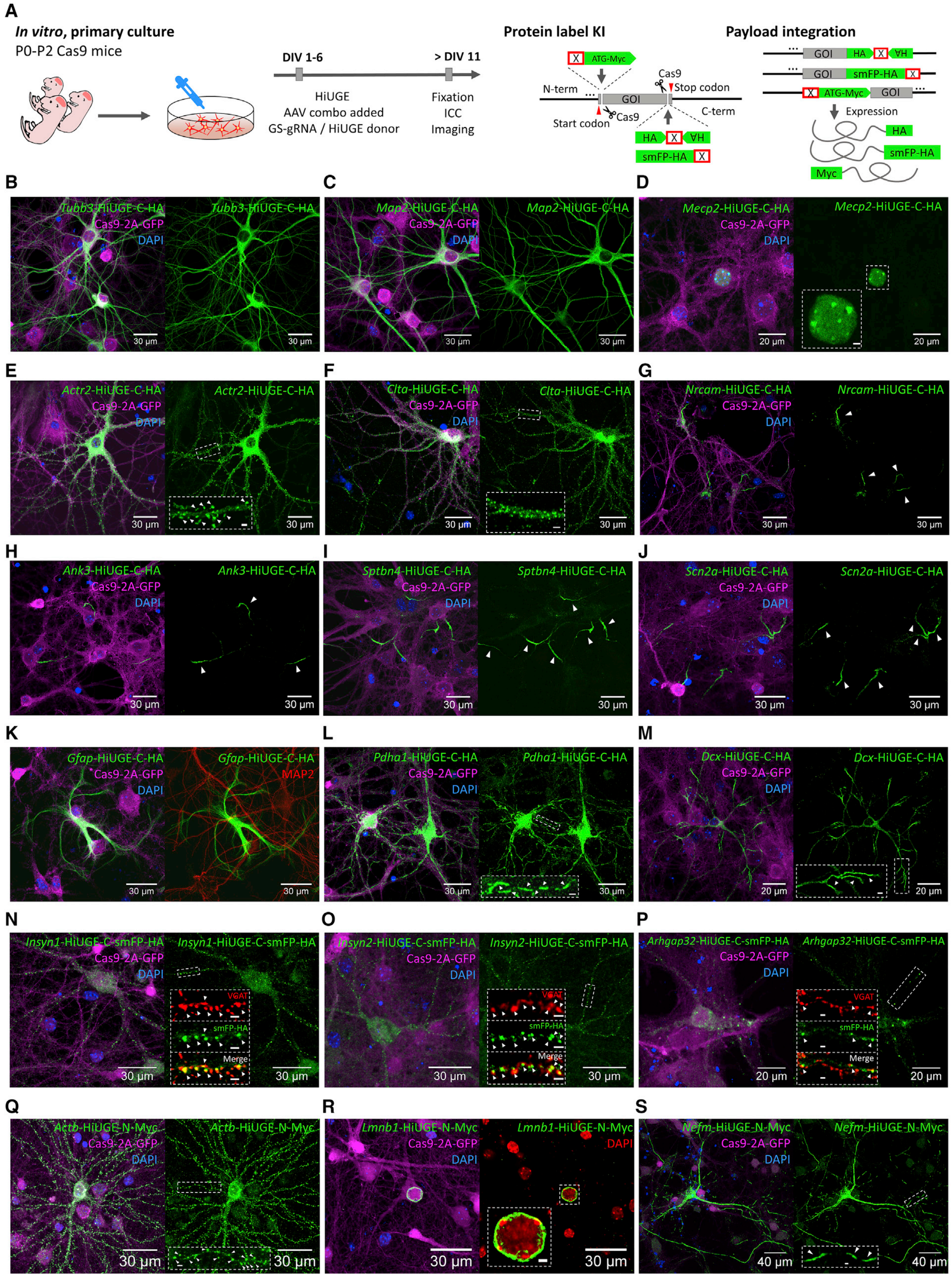
A
In vitro, primary culture
P0-P2 Cas9 mice
DIV 1-6
> DIV 11
HiUGE
AAV combo added
GS-gRNA / HiUGE donor
Fixation
ICC
Imaging
Protein label KI
ATG-Myc
N-term
GOI
Cas9
Stop codon
C-term
Start codon
Cas9
HA
smFP-HA
Payload integration
GOI
HA
smFP-HA
ATG-Myc
Expression
HA
smFP-HA
Myc
B
Tubb3-HiUGE-C-HA
Cas9-2A-GFP
DAPI
30 µm
C
Map2-HiUGE-C-HA
D
Mecp2-HiUGE-C-HA
20 µm
E
Actr2-HiUGE-C-HA
F
Clta-HiUGE-C-HA
G
Nrcam-HiUGE-C-HA
H
Ank3-HiUGE-C-HA
I
Sptbn4-HiUGE-C-HA
J
Scn2a-HiUGE-C-HA
K
Gfap-HiUGE-C-HA
MAP2
L
Pdha1-HiUGE-C-HA
M
Dcx-HiUGE-C-HA
N
Insyn1-HiUGE-C-smFP-HA
VGAT
smFP-HA
Merge
O
Insyn2-HiUGE-C-smFP-HA
P
Arhgap32-HiUGE-C-smFP-HA
Q
Actb-HiUGE-N-Myc
R
Lmnb1-HiUGE-N-Myc
DAPI
S
Nefm-HiUGE-N-Myc
40 µm

(legend on next page)

et al., 1999; Gdalyahu et al., 2004). Colony screening demonstrated that the cloning reactions were highly efficient (Figures S1F–S1H). Primary neuron-glia cultures of Cas9 mice were co-transduced with one of these GS-gRNA AAVs in combination with the same HA-epitope donor AAV (Figure 2A). Approximately 7 days following infection, we observed the predicted localization of the 12 protein targets by HA immunostaining (Figures 2B–2M). Further, genomic PCRs were performed for five targets to amplify the region around the edited junctions. HA-epitope integrations were confirmed (Figures S3A and S3B), with deep sequencing of the amplicons revealing the positional indel occurrences, the proportions of forward and reverse payload insertion without indels, and the proportions of allelic mutations without donor integration (Figure S3C). We also tested for the integration of donor payloads in top-ranked predicted off-target sites and found no evidence for payload insertion (Figures S3D and S3E). In addition, experimental genome-wide analysis was performed to detect potential off-target payload integrations, including those at non-predicted sites. We found that while genomic off-target integrations can occur, their estimated frequencies are low (Figures S3F–S3H). In each instance, the observed off-target integration was into non-coding regions that would not result in unintended labeling of non-target proteins. Further, the cellular labeling efficiencies across various conditions were quantified for several AIS-specific targets, as each neuron typically has only one AIS, and their distinct expression pattern is suitable for easy visual identification and quantification. The ratios of HiUGE-labeled AIS structures compared to all AIS (stained with an antibody against the AIS-marker Ankyrin-G) were quantified (Figures S4A–S4C). Estimated efficiencies were shown across multiple viral doses (*Sptbn4*: 34%; *Scn2a*: 29% at the high dose) and across various ratios between the GS-gRNA and the donor (ratios around 1:1 are optimal). Further, we tested HiUGE-mediated labeling to visualize several members of the recently uncovered inhibitory postsynaptic density (iPSD) proteome (Uezu et al., 2016). Spaghetti-monster HA (smFP-HA), a larger insert that exhibits enhanced antigenicity suitable for detecting low-expression proteins (Viswanathan et al., 2015), was used as the payload (Figure 2A). These iPSD proteomic candidates included inhibitory synaptic protein 1 (*Insyn1*), inhibitory synaptic protein 2 (*Insyn2*), and Rho GTPase activating protein 32 (*Arhgap32*). Immunocytochemistry demonstrated that they were localized juxtaposed to the vesicular GABA transporter (VGAT) (Figures 2N–2P), confirming their presence at inhibitory synapses. In addition, three different GS-gRNAs (Table S1) were tested for *Insyn1*, and all of them yield comparable inhibitory synaptic labeling (Figures S4D–S4G), demonstrating the flexibility of GS-gRNA selection and the robustness of the labeling method. Finally, we performed mixed labeling of diverse protein targets by applying a single C-term HA-epitope donor with a mixture of GS-gRNA AAVs (Figures S4H and S4I). Immunocytochemistry revealed simultaneous labeling of the targeted proteins (βIV-spectrin, GFAP, and MeCP2) in a single experiment and provided a proof of concept for other applications that require simultaneous modification of multiple proteins.

Next, we tested N-term modifications using a single Myc-epitope payload with an upstream stop codon cassette to constrain its expression to the N-term (Figure 2A). GS-gRNAs targeting the N-term of three proteins were tested, including proteins of the actin cytoskeleton (β-actin, *Actb*), nuclear envelope (lamin B1, *Lmnb1*), and neurofilaments (neurofilament medium, *Nefm*). Myc-epitope immunolabeling, consistent with the expected localization pattern, was observed for each target (Figures 2Q–2S). Further, like previous studies (Mikuni et al., 2016), we tested selective dual labeling of different proteins with different tags. This is achieved by combining the N-term selective Myc-epitope payload with the HA-epitope HiUGE payload described above, which contains a stop codon cassette following the epitope tag that enforces its expression at the C-term (Figure S4J). These donors were co-infected with GS-gRNA AAVs targeting the N-term of dendritic MAP2 (*Map2*) and the C-term of AIS-enriched βIV-spectrin (*Sptbn4*). Co-staining for HA and Myc-epitopes revealed selective labeling for each protein, with instances of co-staining in single neurons (Figure S4K). Thus, HiUGE N- and C-term selective payloads can be used to co-label proteins simultaneously to reveal the spatial relationships of two endogenous proteins, which may be more useful than the mixed labeling of multiple proteins with identical tags described above.

Together, using rapidly constructed GS-gRNA libraries, HiUGE integrates universal payloads into diverse protein coding regions in a highly specific and higher-throughput manner for mapping endogenous protein localizations. HiUGE is thus suitable for rapid and robust labeling of proteins, including post hoc localization analysis following large-scale proteomic studies.

In Vivo HiUGE Labeling of Proteins via Viral Delivery

We next tested *in vivo* labeling by intracranial injections of HiUGE AAVs (Figure 3A). Approximately 2 weeks following infection, immunohistochemistry was performed. Images of sections from each injection revealed the expected HA immunoreactivity localized to the AIS (*Sptbn4* and *Scn2a*; Figures 3B and 3C),

Figure 2. Rapid Protein Modification across Diverse Genomic and Protein Targets with HiUGE *In Vitro*

(A) Schematic of HiUGE KI application for C- or N-term protein labeling *in vitro*. Primary hippocampal cells from Cas9 mice were transduced with a combination of GS-gRNA and HiUGE donor AAVs and immunostained to detect epitope or smFP-HA labeling, with representative images displayed in (B)–(S).

(B–M) Examples of C-term HA-epitope KI to diverse targets (mouse *Tubb3*, B; *Map2*, C; *Mecp2*, D; *Actr2*, E; *Clta*, F; *Nrcam*, G; *Ank3*, H; *Sptbn4*, I; *Scn2a*, J; *Gfap*, K; *Pdha1*, L; and *Dcx*, M), showing the expected expression patterns of the translated proteins, respectively.

(N–P) C-term smFP-HA KI to mouse *Insyn1* (N), *Insyn2* (O), and *Arhgap32* (P), which encode the inhibitory postsynaptic density (iPSD) proteomic candidates. Colocalization of the HA-immunoreactivity with the juxtaposed inhibitory presynaptic marker vesicular GABA transporter (VGAT) immunosignal is shown in the insets.

(Q–S) N-term Myc-epitope KI to mouse *Actb* (Q), *Lmnb1* (R), and *Nefm* (S), showing the expected expression patterns of the translated proteins respectively.

Scale bar is indicated in each panel or within insets (2 μm). GFP fluorescence of the Cas9-2A-GFP and nuclei labeling with DAPI are also shown. Arrowheads represent the subcellular features associated with the targeted genes, such as the dendritic spines, AIS, mitochondria, distal end of neurites, inhibitory synapses, and neurofilaments.

Please cite this article in press as: Gao et al., Plug-and-Play Protein Modification Using Homology-Independent Universal Genome Engineering, Neuron (2019), https://doi.org/10.1016/j.neuron.2019.05.047

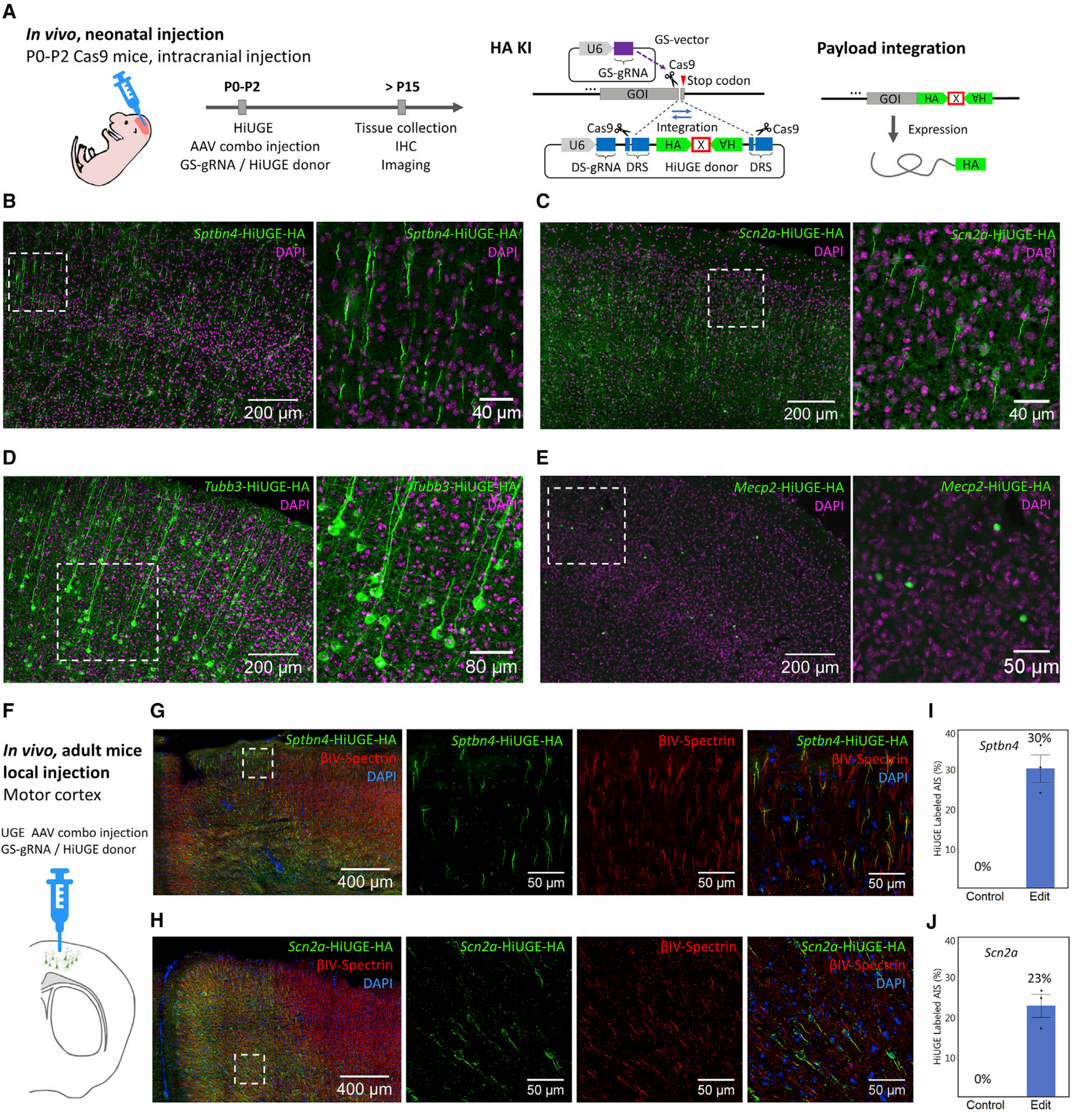
A
In vivo, neonatal injection
P0-P2 Cas9 mice, intracranial injection
P0-P2
> P15
HiUGE
AAV combo injection
GS-gRNA / HiUGE donor
Tissue collection
IHC
Imaging
HA KI
U6
GS-vector
GS-gRNA
Cas9
Stop codon
GOI
Integration
Cas9
Cas9
U6
HA
X
HA
DS-gRNA
DRS
HiUGE donor
DRS
Payload integration
GOI
HA
X
HA
Expression
HA
B
Sptbn4-HiUGE-HA
DAPI
200 μm
40 μm
C
Scn2a-HiUGE-HA
DAPI
200 μm
40 μm
D
Tubb3-HiUGE-HA
DAPI
200 μm
80 μm
E
Mecp2-HiUGE-HA
DAPI
200 μm
50 μm
F
In vivo, adult mice
local injection
Motor cortex
HiUGE AAV combo injection
GS-gRNA / HiUGE donor
G
Sptbn4-HiUGE-HA
βIV-Spectrin
DAPI
400 μm
50 μm
50 μm
50 μm
H
Scn2a-HiUGE-HA
βIV-Spectrin
DAPI
400 μm
50 μm
50 μm
50 μm
I
Sptbn4
HiUGE Labeled AIS (%)
40
30
20
10
0%
30%
Control
Edit
J
Scn2a
HiUGE Labeled AIS (%)
40
30
20
10
0%
23%
Control
Edit

Figure 3. Endogenous Protein Labeling with HiUGE *In Vivo*

(A) Schematic of C-term HA-epitope KI *in vivo*. Neonatal Cas9 pups were intracranially injected with a combination of purified GS-gRNA AAV and HiUGE donor AAV and euthanized after P15 for immunohistochemistry to detect HA-epitope KI.

(B–E) Representative images of HA-epitope KI to mouse *Sptbn4* (B), *Scn2a* (C), *Tubb3* (D), and *Mecp2* (E), showing the expected expression patterns of the translated proteins, respectively. Cortical regions of coronal sections are shown. Image on the right within each panel shows a magnified view of the boxed region from the left image.

(F) Adult Cas9 mice were locally injected with a combination of purified GS-gRNA and HA-epitope donor AAVs (titer of 3 × 10^{10} GC/μL) into the motor cortex and euthanized 2 weeks later for immunohistochemistry.

(G and H) Representative immunofluorescent images of HA-epitope (green) following HiUGE-mediated KI to mouse *Sptbn4* (G) and *Scn2a* (H). Antibody labeling of the AIS-marker (βIV-spectrin) is also shown (red).

(I and J) Quantification of cellular labeling efficiency showing the fractions of the βIV-spectrin-positive AIS-structures labeled with HiUGE at the injection sites (*Sptbn4*, I: 30.2% ± 3.4%; *Scn2a*, J: 22.8% ± 2.9%, n = 3 mice), in comparison to negative controls (uninjected, 0%).

Error bars represent SEM. Scale bar is indicated in each panel.

Please cite this article in press as: Gao et al., Plug-and-Play Protein Modification Using Homology-Independent Universal Genome Engineering, Neuron (2019), https://doi.org/10.1016/j.neuron.2019.05.047

microtubules (*Tubb3*; Figure 3D), and nuclei (*Mecp2*; Figure 3E). Of note, the detection for each of four targets was consistent across independent cells with no visible mis-localization, suggesting off-target protein coding integration was undetectable or rare. In addition, local injections of HiUGE AAVs into the motor cortex of adult Cas9 mice were performed, and the cellular labeling efficiencies for the AIS-localized targets at the injection sites were quantified (*Sptbn4*: 30%; *Scn2a*: 23%. Figures 3F–3J). These data demonstrated that a single HiUGE donor can be paired with multiple GS-gRNAs to modify diverse endogenous proteins *in vivo*.

Multiplex Labeling Demonstrates HiUGE Donor Payloads Are Interchangeable at Single Genomic Locus

While the above data demonstrated that a single HiUGE payload could integrate across diverse gene targets *in vitro* and *in vivo*, an additional feature of the HiUGE method is that the donor payloads should be interchangeable for multiplexing and flexible selection of protein modifications. The ability to mix and match premade HiUGE donors would simplify the experimental selection of optimal epitopes, diverse fusion proteins, or fusion proteins with variable linkers. To demonstrate the interchangeability of HiUGE payloads, we modified proteins either *in vitro* or *in vivo* with a combination of epitope tags (HA, Myc, and/or V5) to create a mosaic labeling of infected cells (Figure 4A). Immunostaining of cultured neurons infected with a mixture of these HiUGE epitope payload AAVs paired with GS-gRNA AAV targeting the *Tubb3* locus revealed a visual montage of multicolored βIII-tubulin labeling, with occasional double-labeled cells indicating the two alleles of *Tubb3* were modified by different epitopes (Figure 4B, magenta neurons). Thus, after genomic cleavage directed by the GS-gRNA, different HiUGE payloads can be inserted interchangeably. Further, multiplexed labeling was also tested *in vivo*, where a mixture of HiUGE epitope payload AAVs were co-injected with the *Tubb3* GS-gRNA AAV into neonatal pups intracranially. Two weeks following infections, immunohistochemistry revealed extensive multiplexed labeling of neurons throughout multiple brain regions of the cerebrum (Figure 4C). Higher magnification images (Figure 4D) demonstrated heterogeneous epitope labeling of ßIII-tubulin in neighboring neurons of the cortex, hippocampus, and thalamus, as well as projections representing thalamocortical connectivity, globus pallidus bundles, and corpus callosum fibers. Together, these data demonstrated the interchangeability of HiUGE donor payloads within a single gene locus, thus enabling flexible selection of diverse protein modifications.

Neural-Circuit-Based HiUGE Payload Delivery

We further reasoned that it should be possible to limit the genome editing activity to specific neural circuits by utilizing a recently reported retrograde-transported AAV2-retro serotype (Tervo et al., 2016). Injection of AAV2-retro GS-gRNA into a brain area containing axon terminals of a circuit could be paired with injection of AAV2/9 HiUGE donor into a specific projection region, allowing retrograde access of projection neurons from a target brain region for neural circuit-selective protein manipulations. We tested this possibility in the well-defined cortico-striatal circuit and the thalamocortical circuit. For the corticostriatal circuit, *Tubb3* GS-gRNA AAV2-retro was injected to the striatum, whereas individual AAV2/9 HiUGE donor AAVs were injected laterally into either the primary motor cortex (MOp, HA-epitope) or secondary motor cortex (MOs, Myc-epitope) of adult conditional Cas9 mice (Figure 5A). Retrograde access to the projection neurons in the motor cortex was confirmed by positive GFP labeling, indicating Cre-dependent activation of Cas9-2A-GFP (Figure 5B). HiUGE-edited projection neurons within the motor cortex were clearly delineated by HA- and Myc-epitope-labeled βIII-tubulin, corresponding to the injection sites (Figures 5C and 5D). Bundles of GFP-positive fibers were also observed in the striatum representing corticostriatal projections (Figures 5E and 5F). Individual axons immunopositive for either the HA or Myc-epitope, which presumably originated from neurons of different motor cortical subregions, were present within neighboring corticostriatal axon bundles (Figures 5G and 5H). Similar circuit-selective HA-epitope tagging of ßIII-tubulin within thalamic projection neurons was also observed in the thalamocortical circuit (Figures 5I–5K). Thus, retrograde infection of projection neurons with AAV2-retro enabled HiUGE-mediated protein modification specific to neural circuit connectivity.

Diverse HiUGE Payloads Enable Approaches to Study Endogenous Protein Dynamics and Functions

Modification of endogenous proteins in mammalian cells in order to delineate their physiological functions is a highly promising area of CRISPR-genome editing. Leveraging the "plug-and-play" interchangeability of HiUGE payloads, we tested various payload sequences for studying the dynamics and functions of endogenous proteins.

Fluorescent proteins (FPs) are commonly used for imaging protein localization and dynamics. However, conventional experiments usually rely on exogenic overexpression of fusions that are susceptible to artifacts associated with the elevated expression levels. To test HiUGE-mediated KI of fluorescent proteins to label endogenously expressed proteins, the coding sequence for mCherry (Shaner et al., 2004) containing a flexible linker was used as the payload to tag several genes (Figure 6A), including mouse *Tubb3* (Figure 6B), *Gfap* (Figure 6C), and *Pdha1* (Figure 6D). HiUGE-mediated KI of mCherry was readily visualized by either immunostaining (Figure 6B) or direct fluorescence (Figures 6C and 6D). A similar labeling pattern was also observed using a mCherry donor without the flexible linker (Figures S4L and S4M). If desired, donor vectors with or without linkers can be paired with panels of GS-gRNA vectors to rapidly optimize the labeling strategy. Further, HiUGE-mediated mCherry labeling was also sufficient for live imaging (Video S1), showing the dynamics of mitochondria following KI of mCherry into mouse *Pdha1*. Together, HiUGE-mediated KI of fluorescent proteins can facilitate dynamic visualization of endogenous proteins.

As proper localization is key to the physiological actions of proteins, one mechanism to alter protein function is to manipulate their subcellular residency with exogenous localization tags (Bear et al., 2000; Niopek et al., 2014). A classic example is the nuclear localization signal (NLS) from SV40 T-antigen that targets proteins into the nucleus via importins (Kalderon et al., 1984; Kosugi et al., 2009; Lange et al., 2007). Here, we chose Arp2 (*Actr2*), an actin-regulating protein that is normally

Please cite this article in press as: Gao et al., Plug-and-Play Protein Modification Using Homology-Independent Universal Genome Engineering, Neuron (2019), https://doi.org/10.1016/j.neuron.2019.05.047

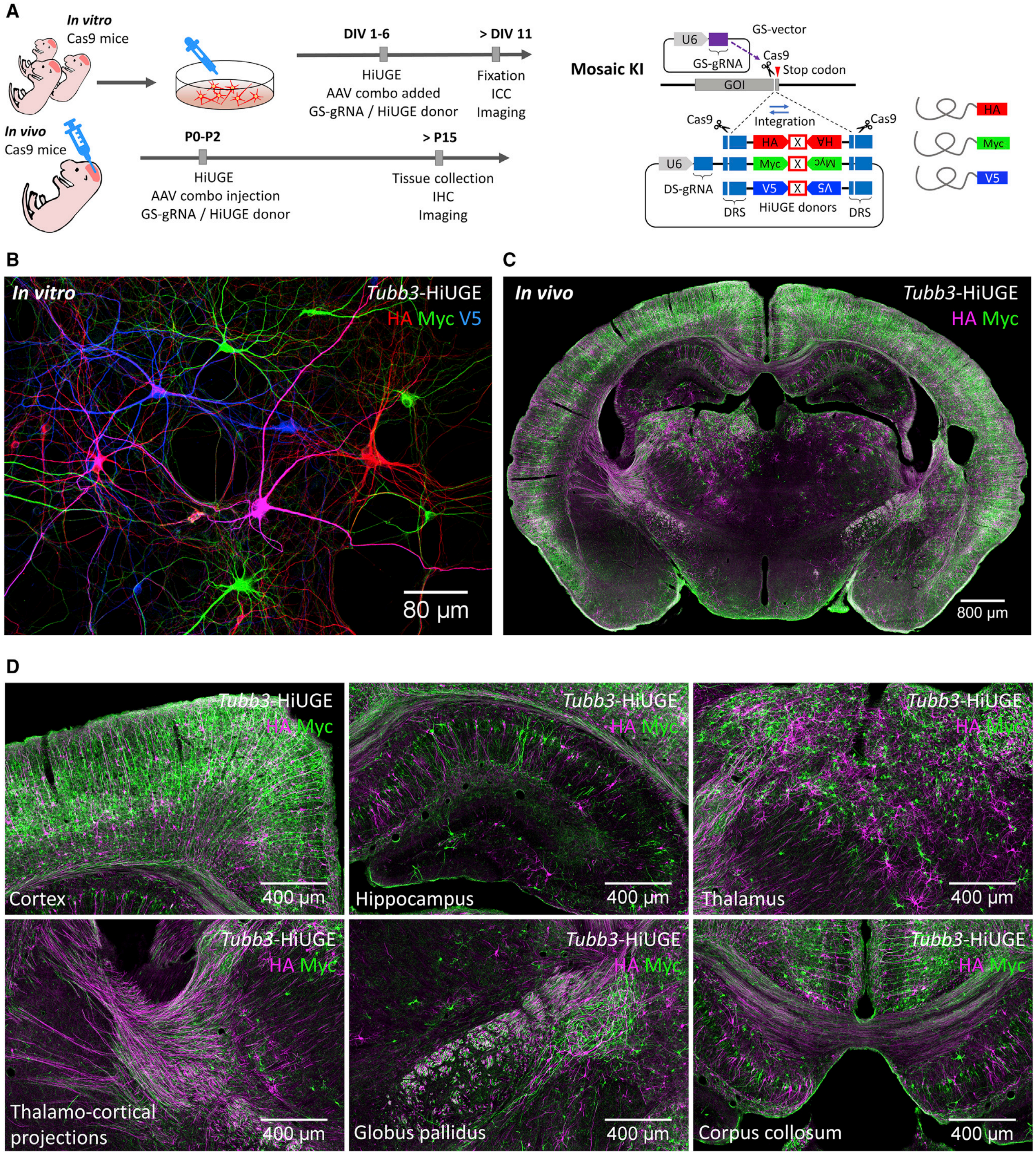
A
In vitro
Cas9 mice
DIV 1-6
> DIV 11
HiUGE
AAV combo added
GS-gRNA / HiUGE donor
Fixation
ICC
Imaging
In vivo
Cas9 mice
P0-P2
> P15
HiUGE
AAV combo injection
GS-gRNA / HiUGE donor
Tissue collection
IHC
Imaging
Mosaic KI
U6
GS-gRNA
GS-vector
Cas9
Stop codon
GOI
Cas9
Integration
Cas9
HA
X
HA
U6
Myc
X
Myc
DS-gRNA
V5
X
V5
DRS
HiUGE donors
DRS
HA
Myc
V5
B
In vitro
Tubb3-HiUGE
HA Myc V5
80 μm
C
In vivo
Tubb3-HiUGE
HA Myc
800 μm
D
Tubb3-HiUGE
HA Myc
Cortex
400 μm
Hippocampus
Thalamus
Thalamo-cortical projections
Globus pallidus
Corpus collosum

Figure 4. HiUGE Donor Payload Interchangeability for Multiplexed Protein Modification

(A) Schematic of C-term KI of epitope mixture *in vitro* and *in vivo*.

(B) Labeling of HA, Myc, and V5-epitope following mosaic KI to mouse *Tubb3*, showing stochastically integrated epitopes in neighboring neurons *in vitro*. Occasionally, cells positive for two epitopes can be seen (e.g., the magenta-colored cell in this image, showing both HA and V5 immunoreactivity).

(C) Coronal section demonstrating labeling of HA and Myc-epitope following mosaic KI to mouse *Tubb3 in vivo.*

(D) Zoomed images showing the cortex, hippocampus, thalamus, thalamocortical projections, globus pallidus, and corpus collosum of (C).

Scale bar is indicated in each panel.

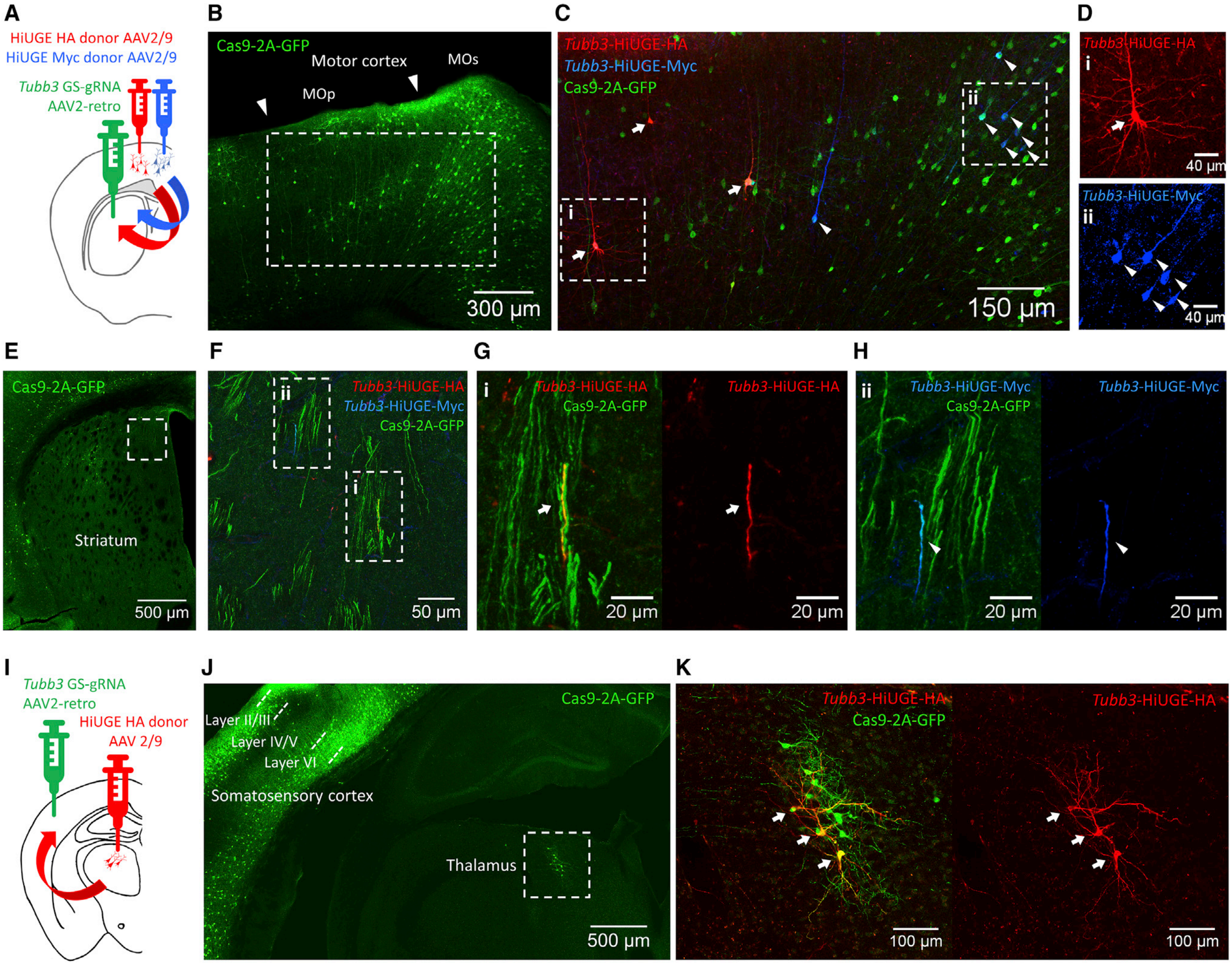
A
HiUGE HA donor AAV2/9
HiUGE Myc donor AAV2/9
Tubb3 GS-gRNA
AAV2-retro
B
Cas9-2A-GFP
Motor cortex
MOs
MOp
300 μm
C
Tubb3-HiUGE-HA
Tubb3-HiUGE-Myc
Cas9-2A-GFP
ii
i
150 μm
D
Tubb3-HiUGE-HA
i
40 μm
Tubb3-HiUGE-Myc
ii
40 μm
E
Cas9-2A-GFP
Striatum
500 μm
F
ii
i
Tubb3-HiUGE-HA
Tubb3-HiUGE-Myc
Cas9-2A-GFP
50 μm
G
i
Tubb3-HiUGE-HA
Cas9-2A-GFP
20 μm
Tubb3-HiUGE-HA
20 μm
H
ii
Tubb3-HiUGE-Myc
Cas9-2A-GFP
20 μm
Tubb3-HiUGE-Myc
20 μm
I
Tubb3 GS-gRNA
AAV2-retro
HiUGE HA donor
AAV 2/9
J
Cas9-2A-GFP
Layer II/III
Layer IV/V
Layer VI
Somatosensory cortex
Thalamus
500 μm
K
Tubb3-HiUGE-HA
Cas9-2A-GFP
100 μm
Tubb3-HiUGE-HA
100 μm

Figure 5. Neural Circuit-Based HiUGE Labeling

(A) Illustration of corticostriatal circuit-selective C-term labeling of ßIII-tubulin by injection of AAV2-retro mouse *Tubb3* GS-gRNA into the striatum and two lateral injections of AAV2/9 HA and Myc-epitope donors in the motor cortex.

(B) Representative image showing GFP labeling in the motor cortex, indicating retrogradely accessed Cre-dependent Cas9-2A-GFP expression in projection neurons.

(C) Immunolabeling of HA- (arrows) and Myc-epitope (arrowheads)-tagged ßIII-tubulin, imaged from the boxed area in (B).

(D) Enlarged images from the boxed areas in (C), showing cells positive for (i) HA or (ii) Myc-epitope.

(E) GFP signal from the AAV2-retro-injected striatum.

(F) Zoomed image of the boxed area in (E), showing GFP-positive axon bundles that contain fibers positive for HA or Myc-epitope.

(G and H) Enlarged images showing fibers positive for (G, i) HA or (H, ii) Myc-epitope within GFP-positive axon bundles from boxed areas in (F).

(I) Illustration of thalamocortical circuit-selective C-term labeling of ßIII-tubulin by injection of AAV2-retro mouse *Tubb3* GS-gRNA in the somatosensory cortex and injection of AAV2/9 HA-epitope donor in the thalamus.

(J) Representative image showing retrogradely activated Cas9-2A-GFP expression within the thalamus (boxed area) and local cortical networks (mostly cells within layer II-III and layer VI).

(K) Zoomed image of the boxed area in (J) showing retrogradely accessed and HiUGE-edited thalamic neurons positive for HA-epitope (arrows) and Cas9-2A-GFP.

Scale bar is indicated in each panel.

enriched in dendritic spines to exemplify subcellular rerouting and sequestration using HiUGE. A dual-orientation HA-NLS HiUGE payload (Figure 6E) was targeted to the C terminus of mouse Arp2 to determine if this cytoskeletal protein could be relocated to the nucleus (Figure 6F). Neurons were transduced with mouse *Actr2* GS-gRNA AAV and a mixture of HA-NLS and Myc-epitope (no NLS) HiUGE payloads. HA-NLS-tagged Arp2 (red) was completely redirected to the nuclei, whereas the Myc-tagged Arp2 (green) was mostly found in the dendritic spines, the normal localization of Arp2 (Figure 6G). Thus, HiUGE

Please cite this article in press as: Gao et al., Plug-and-Play Protein Modification Using Homology-Independent Universal Genome Engineering, Neuron (2019), https://doi.org/10.1016/j.neuron.2019.05.047

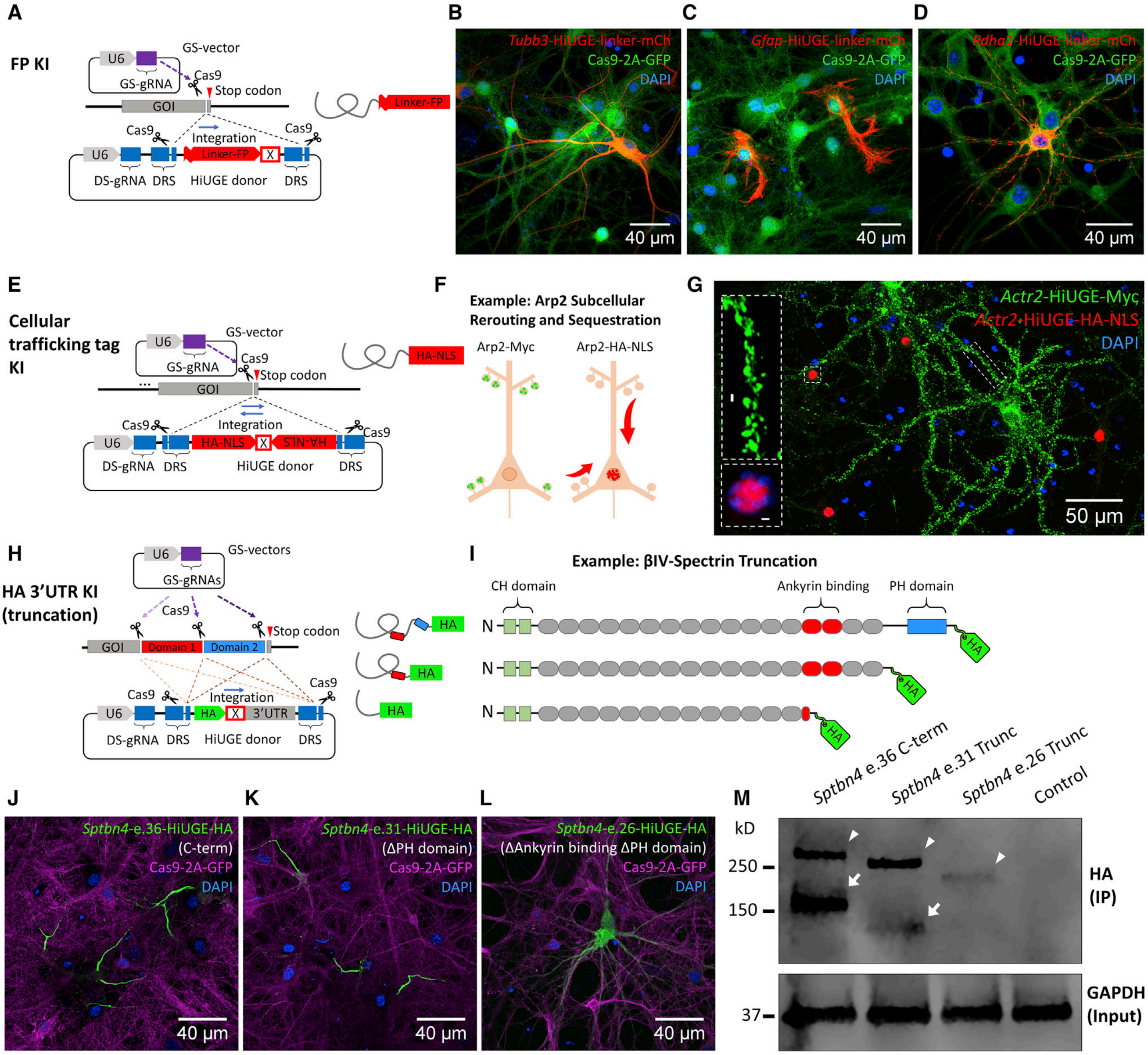
A
FP KI
U6
GS-vector
GS-gRNA
Cas9
Stop codon
GOI
Linker-FP
Cas9
Integration
Cas9
U6
Linker-FP
X
DS-gRNA
DRS
HiUGE donor
DRS
B
Tubb3-HiUGE-linker-mCh
Cas9-2A-GFP
DAPI
40 μm
C
Gfap-HiUGE-linker-mCh
Cas9-2A-GFP
DAPI
40 μm
D
Pdha1-HiUGE-linker-mCh
Cas9-2A-GFP
DAPI
40 μm
E
Cellular trafficking tag KI
U6
GS-vector
GS-gRNA
Cas9
Stop codon
GOI
HA-NLS
Cas9
Integration
Cas9
U6
HA-NLS
X
HA-NLS
DS-gRNA
DRS
HiUGE donor
DRS
F
Example: Arp2 Subcellular Rerouting and Sequestration
Arp2-Myc
Arp2-HA-NLS
G
Actr2-HiUGE-Myc
Actr2-HiUGE-HA-NLS
DAPI
50 μm
H
HA 3′UTR KI (truncation)
U6
GS-vectors
GS-gRNAs
Cas9
Stop codon
GOI
Domain 1
Domain 2
HA
HA
HA
Cas9
Cas9
Integration
U6
HA
X
3′UTR
DS-gRNA
DRS
HiUGE donor
DRS
I
Example: βIV-Spectrin Truncation
CH domain
Ankyrin binding
PH domain
N
HA
N
HA
N
HA
J
Sptbn4-e.36-HiUGE-HA (C-term)
Cas9-2A-GFP
DAPI
40 μm
K
Sptbn4-e.31-HiUGE-HA (ΔPH domain)
Cas9-2A-GFP
DAPI
40 μm
L
Sptbn4-e.26-HiUGE-HA (ΔAnkyrin binding ΔPH domain)
Cas9-2A-GFP
DAPI
40 μm
M
Sptbn4 e.36 C-term
Sptbn4 e.31 Trunc
Sptbn4 e.26 Trunc
Control
kD
250
150
37
HA (IP)
GAPDH (Input)

Figure 6. HiUGE Payloads Enable Flexible Selection across Multiple Methods to Interrogate Endogenous Protein Functions

(A) Schematic of fluorescent protein KI with flexible (GGGGS)$_4$ linker.

(B–D) Detection of mCherry (mCh) KI to different genomic targets (mouse *Tubb3*, *Gfap*, and *Pdha1*) with (B) antibody against mCh, or (C and D) direct visualization of mCh fluorescence.

(E) Schematic of HiUGE subcellular rerouting constructs using cellular trafficking tags as the payloads.

(F) Example using a HiUGE payload with HA-epitope and nuclear localization signal (HA-NLS) to sequester an actin cytoskeletal protein Arp2 to the nucleus.

(G) Representative image of immunostaining following C-term HA-NLS KI to mouse *Actr2* gene showing the HA-NLS-tagged Arp2 (red) redirected to the nucleus. Simultaneously, the Myc-epitope (no NLS) tagged Arp2 (green) was enriched at the dendritic spines, consistent with the normal localization of Arp2.

(H) Schematic illustration of HiUGE HA-3′ UTR KI to truncate endogenous proteins for conducting structure-function relationship studies.

(I) Example using HA-3′ UTR KI strategy to truncate βIV spectrin, composed of calponin homology (CH) domains, spectrin repeats, and a pleckstrin homology (PH) domain.

(J–L) C-term KI using a GS-gRNA targeting near the stop codon of the last coding exon 36 (e.36) of βIV-spectrin (J) is compared to truncation of PH domain by targeting exon 31 (e.31) (K), which still retains AIS enrichment, or disruption of spectrin repeat 14 and truncation of downstream sequences by targeting exon 26 (e.26) (L), which completely disrupts the AIS localization.

(M) Western blot of HA-epitope showing stepwise reduction of molecular mass consistent with the serial truncation conditions (arrowheads). Arrowheads indicate the ∑1 isoform of βIV-spectrin, while arrows indicate the ∑6 isoform. The ∑6 isoform of the truncation at exon 26 (e.26) appeared undetectable. Molecular mass is marked in reference to the ladder.

Scale bar is indicated in each panel or within insets (2 μm).

payloads of subcellular trafficking tags, such as an NLS, can be harnessed to manipulate the subcellular residency of endogenous proteins for purposes such as loss-of-function or gain-of-function experiments.

Protein truncation experiments are crucial for identifying functional domains, unveiling protein interactions, and delineating structure-function relationships. Once again, conventional methods typically rely on overexpression of exogenic constructs. To enable truncation studies of endogenously expressed proteins, an HA-stop-3′ UTR HiUGE payload was designed (Figure 6H). This construct enables the labeling of truncated endogenous proteins with an epitope while facilitating escape from nonsense-mediated decay by the addition of the 3′ UTR containing a poly-adenylation sequence. This application is exemplified by truncation of ßIV-spectrin, as it is enriched at the AIS and contains modular domain structures (Figure 6I). Pairing the GS-gRNA targeting the last coding exon near the stop codon (exon 36 of the canonical $\sum$1 isoform) resulted in strong HA-epitope immunoreactivity restricted to the AIS (Figure 6J). Targeting exon 31 to delete the pleckstrin homology (PH) domain from ßIV-spectrin did not disrupt its AIS localization (Figure 6K), consistent with previous work suggesting the PH domain is not required for its localization to the AIS (Yang et al., 2007). Remarkably, targeting the more upstream exon 26 to truncate ßIV-spectrin within the 14th spectrin repeat completely abrogated its AIS-enriched immunoreactivity and resulted in a diffuse cytosolic staining (Figure 6L). These results demonstrated that the region between the 14th spectrin repeat and the PH domain of ßIV-spectrin is required for its enrichment within the AIS. This is consistent with previous studies that indicate ßIV-spectrin interacts with the AIS-scaffold protein Ankyrin within the 14th–15th spectrin repeats (Ipsaro et al., 2008; Kennedy et al., 1991; Yang et al., 2007), suggesting this interaction is important for its proper AIS localization. Further, western blot analysis confirmed a stepwise reduction of the protein molecular mass that was consistent with the serial truncation (Figure 6M). Thus, HiUGE enables rapid serial truncation to interrogate structure-function relationships associated with underlying cellular mechanisms.

Together, libraries of HiUGE payloads with different functional moieties facilitate independent approaches to study endogenous proteins. Due to the plug-and-play nature of HiUGE, other DNA sequences, such as an inducible degron tag (Natsume et al., 2016; Nishimura et al., 2009), can also be incorporated as payloads to be delivered to diverse genomic loci, opening a myriad of new possibilities for gene and protein modification and manipulation.

All-in-One HiUGE Vectors Utilizing Intein-Based Cas9 Protein *Trans*-splicing

Thus far, the HiUGE system relies on additional Cas9 expression strategies. To simplify the application in diverse wild-type (WT) cells and animals, we incorporated the sequences for Cas9 expression into the vectors. To overcome the constraint of AAV packaging size, spCas9 was split between the donor and GS-gRNA vectors, with each half incorporating *Npu* split-intein sequences (Cheriyan et al., 2013; Truong et al., 2015). Intein-mediated protein *trans*-splicing would thus enable the reconstitution of full-length spCas9, facilitating HiUGE applications in WT targets (Figures 7A and 7B). This design was tested in WT primary neurons and common cell lines using HA-epitope or GFP payloads paired with GS-gRNAs targeting either mouse *Tubb3*, *Map2*, *Pdha1*, or *Tubb5* genes or human *TUBB* gene. Immunostaining of AAV-transduced neurons showed successful HA-epitope and GFP KI (Figures 7C–7H). Likewise, HiUGE vectors delivered by plasmid co-transfection into common cell lines such as HeLa, HEK293T, and NIH 3T3 also showed successful HA-epitope and GFP KI (Figures 7I–7N). Specificity control experiments showed that the incorporation of the HA-epitope or GFP payloads requires both the GS-gRNA and the donor vectors (Figure S5A). Like the HiUGE system without intein-split-Cas9, we found that around 1:1 ratio between the GS-gRNA and donor is optimal, although a higher overall viral concentration was needed (Figures S5B–S5D). Further, intein-split-Cas9-mediated HiUGE was tested *in vivo*. Purified AAVs targeting mouse *Map2* were unilaterally co-injected into the dorsal hippocampus of adult WT mice. Two weeks after infection, HA-epitope immunostaining revealed robust MAP2 labeling in dendrites and cell bodies within the injected hippocampus, but not on the contralateral uninfected side (Figures 7O and 7P). Together, HiUGE with intein-split-Cas9 simplifies its application in WT cells and animals.

DISCUSSION

Here, we report the development of HiUGE, a simplified approach that allows the flexible targeting of multiple insertional payloads across GOIs to rapidly manipulate and engineer endogenous proteins *in vitro* and *in vivo*. We demonstrate that single HiUGE donor vectors can be used to modify multiple proteins at their C- or N-term and that multiple HiUGE payloads of different functional moieties can be inserted into a single protein. Thus, HiUGE payloads are universal with respect to gene identity, provided that the modifications (insertion of the tag and linker and/or truncation of the terminal amino acids) are functionally tolerated, and retained during post-translational maturation of the protein products (some proteins may be post-translationally processed at both their C- and N-termini, thus inherently difficult to target). Overall, because custom donor vectors to deliver foreign sequences into GOIs are no longer needed, HiUGE dramatically increases the throughput and scalability of localization mapping and functional interrogation of endogenous proteins. To utilize HiUGE, a simple ligation of 23- to 24-mer duplexed oligos into the GS-gRNA backbone vector is sufficient to unlock multiple applications to study gene and protein functions based on homology-independent insertions of diverse HiUGE payloads. Thus, testing different antibody epitopes, fluorescent protein fusions, linker amino acid sequences, and functional modifiers, which are common steps for optimizing protein labeling and manipulation, is easily achievable. Prior methods such as HITI or SLENDR would require additional tailored donor vectors for each optimization strategy. Further, due to the molar excess of oligos, the cloning reaction of GS-gRNA vectors is highly efficient, and easily scalable to tens to hundreds of protein targets by single labs. Moreover, we also note a high success rate for protein labeling during the development of HiUGE (24 genes successful tagged out of 25 tested). We anticipate that HiUGE

Please cite this article in press as: Gao et al., Plug-and-Play Protein Modification Using Homology-Independent Universal Genome Engineering, Neuron (2019), https://doi.org/10.1016/j.neuron.2019.05.047

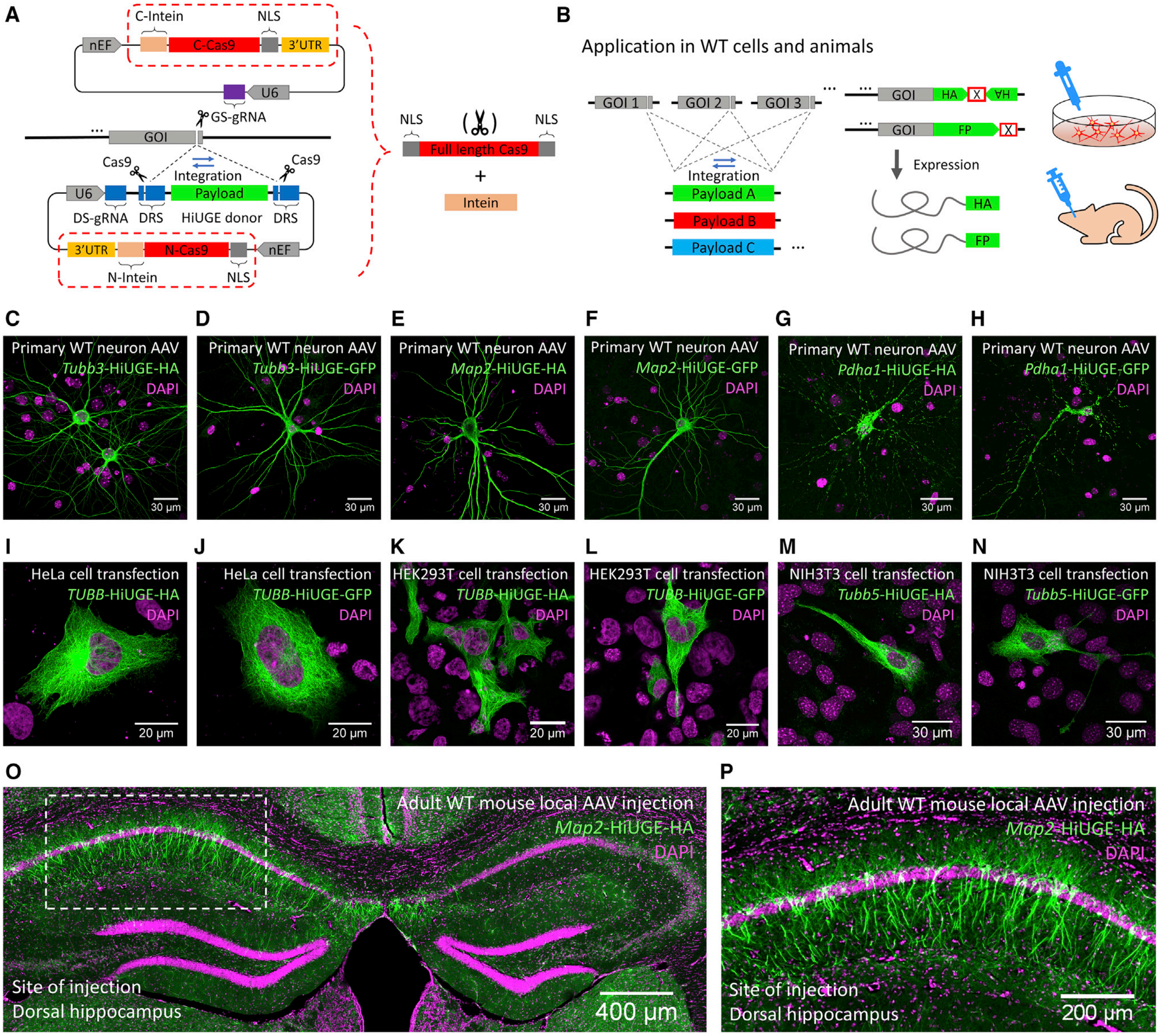
A
C-Intein
NLS
nEF
C-Cas9
3'UTR
U6
GS-gRNA
GOI
Cas9
Integration
Cas9
U6
Payload
DS-gRNA
DRS
HiUGE donor
DRS
3'UTR
N-Cas9
nEF
N-Intein
NLS
NLS
NLS
Full length Cas9
+
Intein
B
Application in WT cells and animals
GOI 1
GOI 2
GOI 3
GOI
HA
X
HA
GOI
FP
X
Integration
Payload A
Payload B
Payload C
Expression
HA
FP
C
Primary WT neuron AAV
Tubb3-HiUGE-HA
DAPI
30 μm
D
Primary WT neuron AAV
Tubb3-HiUGE-GFP
DAPI
30 μm
E
Primary WT neuron AAV
Map2-HiUGE-HA
DAPI
30 μm
F
Primary WT neuron AAV
Map2-HiUGE-GFP
DAPI
30 μm
G
Primary WT neuron AAV
Pdha1-HiUGE-HA
DAPI
30 μm
H
Primary WT neuron AAV
Pdha1-HiUGE-GFP
DAPI
30 μm
I
HeLa cell transfection
TUBB-HiUGE-HA
DAPI
20 μm
J
HeLa cell transfection
TUBB-HiUGE-GFP
DAPI
20 μm
K
HEK293T cell transfection
TUBB-HiUGE-HA
DAPI
20 μm
L
HEK293T cell transfection
TUBB-HiUGE-GFP
DAPI
20 μm
M
NIH3T3 cell transfection
Tubb5-HiUGE-HA
DAPI
30 μm
N
NIH3T3 cell transfection
Tubb5-HiUGE-GFP
DAPI
30 μm
O
Adult WT mouse local AAV injection
Map2-HiUGE-HA
DAPI
Site of injection
Dorsal hippocampus
400 μm
P
Adult WT mouse local AAV injection
Map2-HiUGE-HA
DAPI
Site of injection
Dorsal hippocampus
200 μm

Figure 7. HiUGE Vectors with Intein-Mediated Split-Cas9 *Trans*-splicing

(A) Schematic of the HiUGE system that harbors intein-mediated split-Cas9 expression for use in WT cells and animals.

(B) Illustration of delivering interchangeable payloads to diverse genomic loci using these vectors.

(C–N) Wild-type (WT) primary mouse neurons were AAV transduced (C–H) and common human or mouse cell lines were plasmid transfected (I–N) with combinations of GS-gRNAs and HiUGE donors, followed by immunostaining for HA-epitope or GFP to detect payload KI.

(C, E, and G) Representative images of HA-epitope KI to the mouse *Tubb3*, *Map2*, and *Pdha1* genes showing the expected (C and E) microtubule and (G) mitochondrial localization of the tagged proteins.

(D, F, and H) Representative images of GFP KI to the mouse *Tubb3*, *Map2*, and *Pdha1* genes showing the expected (D and F) microtubule and (H) mitochondrial localization of the tagged proteins.

(I, K, and M) Representative images of HA-epitope KI to the human *TUBB* or mouse *Tubb5* gene showing the expected microtubule localization of the tagged proteins in HeLa cell (I), HEK293T (K), and NIH 3T3 (M) cells.

(J, L, and N) Representative images of GFP KI to the human *TUBB* or mouse *Tubb5* gene showing the expected microtubule localization of the tagged proteins in HeLa (J), HEK293T (L), and NIH 3T3 (N) cells.

(O) Representative image of HA-epitope KI to mouse *Map2* gene following local AAV injection in the dorsal hippocampus of adult WT mice showing efficient labeling of the neurons at the injection site compared to negative labeling on the contralateral side. Zoomed view of the boxed area is shown in (P).

Scale bar is indicated in each panel.

Please cite this article in press as: Gao et al., Plug-and-Play Protein Modification Using Homology-Independent Universal Genome Engineering, Neuron (2019), https://doi.org/10.1016/j.neuron.2019.05.047

will enable higher-throughput mapping and functional interrogation of proteomes, which is urgently needed for analyzing larger-scale proteomic and genomic datasets.

The HiUGE method we outline relies on NHEJ, which has advantages to approaches dependent on HDR. First, while HDR is less frequently observed outside of the S and G2 phases (Heyer et al., 2010; Hsu et al., 2014; Saleh-Gohari and Helleday, 2004), NHEJ repair is operational at all phases of the cell cycle (Mao et al., 2008; Suzuki et al., 2016). Furthermore, quantitative analysis of HDR versus NHEJ suggests the latter is the prevailing repair pathway following DSBs (Mao et al., 2008). Thus, NHEJ-based applications for genome engineering may be more broadly applicable than HDR-dependent approaches. Moreover, dual-orientation design is used for C-term epitope-tag payloads, which allows translation and expression of the tag following both forward and reverse NHEJ-mediated integration. This design maximizes the potential of efficient protein modification and is especially desirable for analyses that require large populations of edited cells. Optimization by testing several GS-gRNAs, which is easy to accomplish with HiUGE, can also be done to identify the most efficient ones.

An important consideration of any CRISPR-based application is the fidelity of genome modification and availability of genomic sites for Cas9-mediated cleavage. One potential drawback to HiUGE, as well as all CRISPR-based approaches, is the formation of indels at the targeted loci. For this reason, phenotypic analysis following these approaches should rely on cells without indels or multiple independent cells to confirm the observation. Rates of indels are likely reduced by the availability of experimental insertional fragments, such as the HiUGE payloads we describe, that disrupt genomic GS-gRNA recognition sites after integration, thus abrogating repetitive rounds of cleavage and repair. Besides, for C-term HiUGE payloads, frameshifting indel events at the integration site abrogate the detectability or reactivity of the translated inserts, thus effectively removing them from the analysis. For N-term fusions, the consistency of labeled proteins across cells is especially important as frameshifting indel events at the integration site could potentially lead to protein depletion and/or the expression of payloads tagged with wrongly encoded peptides in some cells. However, detectable expressions of frameshifted N-term fusions are likely to be very limited due to nonsense-mediated decay triggered by premature stop codons (Baker and Parker, 2004; Hug et al., 2016). Further, off-target insertion of HiUGE payloads can be reduced by computational methods to minimize the selection of gRNAs with potentially high off-target liability (Bae et al., 2014; Haeussler et al., 2016). By genome-wide analysis we found rare off-target integrations of the payload (Figures S3F–S3H). In each instance the integration was into non-coding regions and did not result in unintended labeling of non-target proteins. Additionally, the consistency of protein labeling across cells within an experimental condition demonstrates that the cell-to-cell variability due to off-target integration was minimal enough to prevent detectable expression from non-target coding regions. High-fidelity spCas9 variants, including eSpCas9, SpCas9-HF1, and HypaCas9, are reported to have less off-target tolerance (Chen et al., 2017; Kleinstiver et al., 2016; Slaymaker et al., 2016) and can be incorporated with the HiUGE method to further improve specificity. Likewise, additional variants of spCas9 with less stringent protospacer adjacent motif (PAM) sequence usage, such xCas9 and SpCas9-NG (Hu et al., 2018; Nishimasu et al., 2018), could further increase the flexibility of selecting genomic targets, placing them immediately adjacent to either the natural start or stop sites and minimizing the undesired truncation of terminal amino acids.

We have demonstrated that HiUGE is easily adopted for a variety of applications, exemplified here by (1) localization mapping and dynamic visualization of endogenous proteins, (2) simultaneous N-term and C-term labeling of multiple proteins, (3) targeted rerouting and sequestration of protein subcellular residency, and (4) protein truncation for disrupting its function or performing structure-function relationship analysis. The donor payloads can be interchanged with other custom DNA sequences for additional applications. Further, neighboring neurons within the brain can be heterogeneously modified with diverse payloads, enabling multiplexed labeling that might facilitate lineage tracing or cellular connectomics studies. Moreover, by using AAV2-retro, projection neurons can be retrogradely accessed and edited by HiUGE based on circuit connectivity. This novel approach opens future possibilities for interrogating molecular mechanisms of behaviorally relevant neural circuits with rapid insertional genome engineering.

To generalize HiUGE for applications in WT cells and organisms without relying on Cas9 transgenics, we have shown that the intein-split-Cas9-mediated HiUGE is functional in diverse targets, including multiple cell types, species of origin, and delivery route. We envision that HiUGE can be adapted to broader range of organisms, such as models of avian or aquatic species, by modularly optimizing the following components: (1) the promoter driving gRNA expression, (2) the promoter driving Cas9 expression, (3) Cas9 codon optimization, and (4) viral serotype and delivery route. We also anticipate that cell-type selectivity can be achieved by using selective promoters to restrict Cas9 expression within the cell type of interest, facilitating differential genome modification across diverse subpopulations of cells.

Together, the higher-throughput and modular features of HiUGE to modify endogenous proteins are especially desirable downstream of genomic and proteomic screens that generate hypotheses requiring further analysis. Using HiUGE, we successfully labeled the recently uncovered iPSD proteins Insyn1 and Insyn2, and confirmed their endogenous localization at inhibitory synapses. We anticipate the plug-and-play nature of HiUGE we describe here will facilitate future studies that leverage multiple functionalities to delineate the molecular mechanisms underlying cellular neurobiology.

STAR★METHODS

Detailed methods are provided in the online version of this paper and include the following:

- KEY RESOURCES TABLE
- LEAD CONTACT AND MATERIALS AVAILABILITY
- EXPERIMENTAL MODEL AND SUBJECT DETAILS
    - ○ Gt(ROSA)26Sor$^{tm1(CAG-cas9*,-EGFP)Fezh}$ (Cas9) and C57BL/6J mice

  - ○ Primary mouse hippocampal and cortical neuron / glia culture
  - ○ Cell culture of HEK293T, HeLa, and NIH 3T3 cell lines
- ● METHOD DETAILS
  - ○ Construction of HiUGE Vectors
  - ○ AAV Production
  - ○ Stereotaxic Injections
  - ○ *In Vitro* and *In Vivo* Protein Modification by HiUGE
  - ○ Immunohistochemistry and Immunocytochemistry
  - ○ Microscopic Fluorescence Imaging
  - ○ Western Blot
  - ○ Genomic PCR, TOPO Cloning and DNA Sequencing
  - ○ Assessment of genomic off-target integration
- ● QUANTIFICATION AND STATISTICAL ANALYSIS

SUPPLEMENTAL INFORMATION

Supplemental Information can be found online at https://doi.org/10.1016/j.neuron.2019.05.047.

ACKNOWLEDGMENTS

We thank Drs. Nicolas Devos, David Corcoran, and Jennifer Modliszewski for performing deep sequencing and subsequent bioinformatic analyses. We thank Shataakshi Dube and Riley Mangan for performing stimulated emission depletion (STED) imaging. We thank Drs. Cagla Eroglu and Anne West for their critical reading and comments. This work was supported by NIH grants R01MH103374 (S.H.S.) and R01NS102456 (S.H.S.), a Kahn Neurotechnology Award, and the Duke Bryan Scholar Award (S.H.S.).

AUTHOR CONTRIBUTIONS

Conceptualization, S.H.S. and Y.G.; Methodology, Y.G. and S.H.S.; Investigation, Y.G., E.H., T.W.A.B., E.E., W.E.B., J.L.C., A.U., and Y.X.; Writing – Original Draft, Y.G. and S.H.S.; Writing – Review & Editing, S.H.S., Y.G., E.H., T.W.A.B., E.E., W.E.B., J.L.C., A.U., Y.X., and Y.D.; Funding Acquisition, S.H.S.; Supervision, S.H.S.

DECLARATION OF INTERESTS

S.H.S. and Y.G. have filed a patent application related to this work. S.H.S. is a founder of CasTag Biosciences and a member of its scientific advisory board.

Received: November 6, 2018
Revised: March 13, 2019
Accepted: May 29, 2019
Published: July 1, 2019

REFERENCES

Aurnhammer, C., Haase, M., Muether, N., Hausl, M., Rauschhuber, C., Huber, I., Nitschko, H., Busch, U., Sing, A., Ehrhardt, A., and Baiker, A. (2012). Universal real-time PCR for the detection and quantification of adeno-associated virus serotype 2-derived inverted terminal repeat sequences. Hum. Gene Ther. Methods *23*, 18–28.

Bae, S., Park, J., and Kim, J.S. (2014). Cas-OFFinder: a fast and versatile algorithm that searches for potential off-target sites of Cas9 RNA-guided endonucleases. Bioinformatics *30*, 1473–1475.

Baker, K.E., and Parker, R. (2004). Nonsense-mediated mRNA decay: terminating erroneous gene expression. Curr. Opin. Cell Biol. *16*, 293–299.

Bear, J.E., Loureiro, J.J., Libova, I., Fässler, R., Wehland, J., and Gertler, F.B. (2000). Negative regulation of fibroblast motility by Ena/VASP proteins. Cell *101*, 717–728.

Berglund, L., Björling, E., Oksvold, P., Fagerberg, L., Asplund, A., Szigyarto, C.A., Persson, A., Ottosson, J., Wernérus, H., Nilsson, P., et al. (2008). A genecentric Human Protein Atlas for expression profiles based on antibodies. Mol. Cell. Proteomics *7*, 2019–2027.

Bolger, A.M., Lohse, M., and Usadel, B. (2014). Trimmomatic: a flexible trimmer for Illumina sequence data. Bioinformatics *30*, 2114–2120.

Bradbury, A., and Plückthun, A. (2015). Reproducibility: Standardize antibodies used in research. Nature *518*, 27–29.

Chen, R.Z., Akbarian, S., Tudor, M., and Jaenisch, R. (2001a). Deficiency of methyl-CpG binding protein-2 in CNS neurons results in a Rett-like phenotype in mice. Nat. Genet. *27*, 327–331.

Chen, Z.Y., Yant, S.R., He, C.Y., Meuse, L., Shen, S., and Kay, M.A. (2001b). Linear DNAs concatemerize in vivo and result in sustained transgene expression in mouse liver. Mol. Ther. *3*, 403–410.

Chen, Z.Y., He, C.Y., Ehrhardt, A., and Kay, M.A. (2003). Minicircle DNA vectors devoid of bacterial DNA result in persistent and high-level transgene expression in vivo. Mol. Ther. *8*, 495–500.

Chen, J.S., Dagdas, Y.S., Kleinstiver, B.P., Welch, M.M., Sousa, A.A., Harrington, L.B., Sternberg, S.H., Joung, J.K., Yildiz, A., and Doudna, J.A. (2017). Enhanced proofreading governs CRISPR-Cas9 targeting accuracy. Nature *550*, 407–410.

Cheriyan, M., Pedamallu, C.S., Tori, K., and Perler, F. (2013). Faster protein splicing with the Nostoc punctiforme DnaE intein using non-native extein residues. J. Biol. Chem. *288*, 6202–6211.

Chojnacki, S., Cowley, A., Lee, J., Foix, A., and Lopez, R. (2017). Programmatic access to bioinformatics tools from EMBL-EBI update: 2017. Nucleic Acids Res. *45* (W1), W550–W553.

Cong, L., Ran, F.A., Cox, D., Lin, S., Barretto, R., Habib, N., Hsu, P.D., Wu, X., Jiang, W., Marraffini, L.A., and Zhang, F. (2013). Multiplex genome engineering using CRISPR/Cas systems. Science *339*, 819–823.

Doudna, J.A., and Charpentier, E. (2014). Genome editing. The new frontier of genome engineering with CRISPR-Cas9. Science *346*, 1258096.

Egelhofer, T.A., Minoda, A., Klugman, S., Lee, K., Kolasinska-Zwierz, P., Alekseyenko, A.A., Cheung, M.S., Day, D.S., Gadel, S., Gorchakov, A.A., et al. (2011). An assessment of histone-modification antibody quality. Nat. Struct. Mol. Biol. *18*, 91–93.

Francis, F., Koulakoff, A., Boucher, D., Chafey, P., Schaar, B., Vinet, M.-C., Friocourt, G., McDonnell, N., Reiner, O., Kahn, A., et al. (1999). Doublecortin is a developmentally regulated, microtubule-associated protein expressed in migrating and differentiating neurons. Neuron *23*, 247–256.

Gdalyahu, A., Ghosh, I., Levy, T., Sapir, T., Sapoznik, S., Fishler, Y., Azoulai, D., and Reiner, O. (2004). DCX, a new mediator of the JNK pathway. EMBO J. *23*, 823–832.

Haeussler, M., Schönig, K., Eckert, H., Eschstruth, A., Mianné, J., Renaud, J.B., Schneider-Maunoury, S., Shkumatava, A., Teboul, L., Kent, J., et al. (2016). Evaluation of off-target and on-target scoring algorithms and integration into the guide RNA selection tool CRISPOR. Genome Biol. *17*, 148.

Heyer, W.D., Ehmsen, K.T., and Liu, J. (2010). Regulation of homologous recombination in eukaryotes. Annu. Rev. Genet. *44*, 113–139.

Hogins, J., Crawford, D.C., Zorumski, C.F., and Mennerick, S. (2011). Excitotoxicity triggered by Neurobasal culture medium. PLoS ONE *6*, e25633.

Hsu, P.D., Scott, D.A., Weinstein, J.A., Ran, F.A., Konermann, S., Agarwala, V., Li, Y., Fine, E.J., Wu, X., Shalem, O., et al. (2013). DNA targeting specificity of RNA-guided Cas9 nucleases. Nat. Biotechnol. *31*, 827–832.

Hsu, P.D., Lander, E.S., and Zhang, F. (2014). Development and applications of CRISPR-Cas9 for genome engineering. Cell *157*, 1262–1278.

Hu, J.H., Miller, S.M., Geurts, M.H., Tang, W., Chen, L., Sun, N., Zeina, C.M., Gao, X., Rees, H.A., Lin, Z., and Liu, D.R. (2018). Evolved Cas9 variants with broad PAM compatibility and high DNA specificity. Nature *556*, 57–63.

Hug, N., Longman, D., and Cáceres, J.F. (2016). Mechanism and regulation of the nonsense-mediated decay pathway. Nucleic Acids Res. *44*, 1483–1495.

Please cite this article in press as: Gao et al., Plug-and-Play Protein Modification Using Homology-Independent Universal Genome Engineering, Neuron (2019), https://doi.org/10.1016/j.neuron.2019.05.047

Ipsaro, J.J., Huang, L., Gutierrez, L., and MacDonald, R.I. (2008). Molecular epitopes of the ankyrin-spectrin interaction. Biochemistry *47*, 7452–7464.

Jinek, M., Chylinski, K., Fonfara, I., Hauer, M., Doudna, J.A., and Charpentier, E. (2012). A programmable dual-RNA-guided DNA endonuclease in adaptive bacterial immunity. Science *337*, 816–821.

Jones, S.L., and Svitkina, T.M. (2016). Axon initial segment cytoskeleton: architecture, development, and role in neuron polarity. Neural Plast. *2016*, 6808293.

Kalderon, D., Roberts, B.L., Richardson, W.D., and Smith, A.E. (1984). A short amino acid sequence able to specify nuclear location. Cell *39*, 499–509.

Kennedy, S.P., Warren, S.L., Forget, B.G., and Morrow, J.S. (1991). Ankyrin binds to the 15th repetitive unit of erythroid and nonerythroid beta-spectrin. J. Cell Biol. *115*, 267–277.

Kim, I.H., Racz, B., Wang, H., Burianek, L., Weinberg, R., Yasuda, R., Wetsel, W.C., and Soderling, S.H. (2013). Disruption of Arp2/3 results in asymmetric structural plasticity of dendritic spines and progressive synaptic and behavioral abnormalities. J. Neurosci. *33*, 6081–6092.

Kleinstiver, B.P., Pattanayak, V., Prew, M.S., Tsai, S.Q., Nguyen, N.T., Zheng, Z., and Joung, J.K. (2016). High-fidelity CRISPR-Cas9 nucleases with no detectable genome-wide off-target effects. Nature *529*, 490–495.

Kosugi, S., Hasebe, M., Matsumura, N., Takashima, H., Miyamoto-Sato, E., Tomita, M., and Yanagawa, H. (2009). Six classes of nuclear localization signals specific to different binding grooves of importin alpha. J. Biol. Chem. *284*, 478–485.

Lange, A., Mills, R.E., Lange, C.J., Stewart, M., Devine, S.E., and Corbett, A.H. (2007). Classical nuclear localization signals: definition, function, and interaction with importin alpha. J. Biol. Chem. *282*, 5101–5105.

Lein, E.S., Hawrylycz, M.J., Ao, N., Ayres, M., Bensinger, A., Bernard, A., Boe, A.F., Boguski, M.S., Brockway, K.S., Byrnes, E.J., et al. (2007). Genome-wide atlas of gene expression in the adult mouse brain. Nature *445*, 168–176.

Li, H., and Durbin, R. (2009). Fast and accurate short read alignment with Burrows-Wheeler transform. Bioinformatics *25*, 1754–1760.

Li, H., Handsaker, B., Wysoker, A., Fennell, T., Ruan, J., Homer, N., Marth, G., Abecasis, G., and Durbin, R.; 1000 Genome Project Data Processing Subgroup (2009). The Sequence Alignment/Map format and SAMtools. Bioinformatics *25*, 2078–2079.

Magoč, T., and Salzberg, S.L. (2011). FLASH: fast length adjustment of short reads to improve genome assemblies. Bioinformatics *27*, 2957–2963.

Mali, P., Yang, L., Esvelt, K.M., Aach, J., Guell, M., DiCarlo, J.E., Norville, J.E., and Church, G.M. (2013). RNA-guided human genome engineering via Cas9. Science *339*, 823–826.

Mao, Z., Bozzella, M., Seluanov, A., and Gorbunova, V. (2008). DNA repair by nonhomologous end joining and homologous recombination during cell cycle in human cells. Cell Cycle *7*, 2902–2906.

Martin, M. (2011). Cutadapt removes adapter sequences from high-throughput sequencing reads. EMBnetjournal *17*, 10.

McKenna, A., Hanna, M., Banks, E., Sivachenko, A., Cibulskis, K., Kernytsky, A., Garimella, K., Altshuler, D., Gabriel, S., Daly, M., and DePristo, M.A. (2010). The Genome Analysis Toolkit: a MapReduce framework for analyzing next-generation DNA sequencing data. Genome Res. *20*, 1297–1303.

Michel, M.C., Wieland, T., and Tsujimoto, G. (2009). How reliable are G-protein-coupled receptor antibodies? Naunyn Schmiedebergs Arch. Pharmacol. *379*, 385–388.

Mikuni, T., Nishiyama, J., Sun, Y., Kamasawa, N., and Yasuda, R. (2016). High-throughput, high-resolution mapping of protein localization in mammalian brain by in vivo genome editing. Cell *165*, 1803–1817.

Natsume, T., Kiyomitsu, T., Saga, Y., and Kanemaki, M.T. (2016). Rapid protein depletion in human cells by auxin-inducible degron tagging with short homology donors. Cell Rep. *15*, 210–218.

Niopek, D., Benzinger, D., Roensch, J., Draebing, T., Wehler, P., Eils, R., and Di Ventura, B. (2014). Engineering light-inducible nuclear localization signals for precise spatiotemporal control of protein dynamics in living cells. Nat. Commun. *5*, 4404.

Nishimasu, H., Shi, X., Ishiguro, S., Gao, L., Hirano, S., Okazaki, S., Noda, T., Abudayyeh, O.O., Gootenberg, J.S., Mori, H., et al. (2018). Engineered CRISPR-Cas9 nuclease with expanded targeting space. Science *361*, 1259–1262.

Nishimura, K., Fukagawa, T., Takisawa, H., Kakimoto, T., and Kanemaki, M. (2009). An auxin-based degron system for the rapid depletion of proteins in nonplant cells. Nat. Methods *6*, 917–922.

Nishiyama, J., Mikuni, T., and Yasuda, R. (2017). Virus-mediated genome editing via homology-directed repair in mitotic and postmitotic cells in mammalian brain. Neuron *96*, 755–768.e755.

Pinello, L., Canver, M.C., Hoban, M.D., Orkin, S.H., Kohn, D.B., Bauer, D.E., and Yuan, G.C. (2016). Analyzing CRISPR genome-editing experiments with CRISPResso. Nat. Biotechnol. *34*, 695–697.

Platt, R.J., Chen, S., Zhou, Y., Yim, M.J., Swiech, L., Kempton, H.R., Dahlman, J.E., Parnas, O., Eisenhaure, T.M., Jovanovic, M., et al. (2014). CRISPR-Cas9 knockin mice for genome editing and cancer modeling. Cell *159*, 440–455.

Saleh-Gohari, N., and Helleday, T. (2004). Conservative homologous recombination preferentially repairs DNA double-strand breaks in the S phase of the cell cycle in human cells. Nucleic Acids Res. *32*, 3683–3688.

Schindelin, J., Arganda-Carreras, I., Frise, E., Kaynig, V., Longair, M., Pietzsch, T., Preibisch, S., Rueden, C., Saalfeld, S., Schmid, B., et al. (2012). Fiji: an open-source platform for biological-image analysis. Nat. Methods *9*, 676–682.

Schmid-Burgk, J.L., Höning, K., Ebert, T.S., and Hornung, V. (2016). CRISPaint allows modular base-specific gene tagging using a ligase-4-dependent mechanism. Nat. Commun. *7*, 12338.

Schneider, C.A., Rasband, W.S., and Eliceiri, K.W. (2012). NIH Image to ImageJ: 25 years of image analysis. Nat. Methods *9*, 671–675.

Shaner, N.C., Campbell, R.E., Steinbach, P.A., Giepmans, B.N., Palmer, A.E., and Tsien, R.Y. (2004). Improved monomeric red, orange and yellow fluorescent proteins derived from Discosoma sp. red fluorescent protein. Nat. Biotechnol. *22*, 1567–1572.

Slaymaker, I.M., Gao, L., Zetsche, B., Scott, D.A., Yan, W.X., and Zhang, F. (2016). Rationally engineered Cas9 nucleases with improved specificity. Science *351*, 84–88.

Spence, E.F., and Soderling, S.H. (2015). Actin out: regulation of the synaptic cytoskeleton. J. Biol. Chem. *290*, 28613–28622.

Suzuki, K., Tsunekawa, Y., Hernandez-Benitez, R., Wu, J., Zhu, J., Kim, E.J., Hatanaka, F., Yamamoto, M., Araoka, T., Li, Z., et al. (2016). In vivo genome editing via CRISPR/Cas9 mediated homology-independent targeted integration. Nature *540*, 144–149.

Tervo, D.G., Hwang, B.Y., Viswanathan, S., Gaj, T., Lavzin, M., Ritola, K.D., Lindo, S., Michael, S., Kuleshova, E., Ojala, D., et al. (2016). A designer AAV variant permits efficient retrograde access to projection neurons. Neuron *92*, 372–382.

Truong, D.J., Kühner, K., Kühn, R., Werfel, S., Engelhardt, S., Wurst, W., and Ortiz, O. (2015). Development of an intein-mediated split-Cas9 system for gene therapy. Nucleic Acids Res. *43*, 6450–6458.

Uezu, A., Kanak, D.J., Bradshaw, T.W., Soderblom, E.J., Catavero, C.M., Burette, A.C., Weinberg, R.J., and Soderling, S.H. (2016). Identification of an elaborate complex mediating postsynaptic inhibition. Science *353*, 1123–1129.

Viswanathan, S., Williams, M.E., Bloss, E.B., Stasevich, T.J., Speer, C.M., Nern, A., Pfeiffer, B.D., Hooks, B.M., Li, W.P., English, B.P., et al. (2015). High-performance probes for light and electron microscopy. Nat. Methods *12*, 568–576.

Yang, Y., Ogawa, Y., Hedstrom, K.L., and Rasband, M.N. (2007). betaIV spectrin is recruited to axon initial segments and nodes of Ranvier by ankyrinG. J. Cell Biol. *176*, 509–519.

Ye, J., Coulouris, G., Zaretskaya, I., Cutcutache, I., Rozen, S., and Madden, T.L. (2012). Primer-BLAST: a tool to design target-specific primers for polymerase chain reaction. BMC Bioinformatics *13*, 134.

Zacharias, D.A., Violin, J.D., Newton, A.C., and Tsien, R.Y. (2002). Partitioning of lipid-modified monomeric GFPs into membrane microdomains of live cells. Science *296*, 913–916.

Please cite this article in press as: Gao et al., Plug-and-Play Protein Modification Using Homology-Independent Universal Genome Engineering, Neuron (2019), https://doi.org/10.1016/j.neuron.2019.05.047

STAR★METHODS

KEY RESOURCES TABLE

REAGENT or RESOURCE	SOURCE	IDENTIFIER
Antibodies		
Rat monoclonal anti-HA	Roche/Sigma	Cat#11867423001
Rabbit polyclonal anti-HA	Sigma	Cat#H6908
Mouse monoclonal anti-HA	BioLegend	Cat#MMS-101P
Mouse monoclonal anti-HA Agarose	ThermoFisher (Pierce)	Cat#26181
Rabbit polyclonal anti-Myc	Santa Cruz	Cat#sc-789
Mouse monoclonal anti-V5	ThermoFisher	Cat#R960-25
Chicken polyclonal anti-GFP	Abcam	Cat#ab13970
Rabbit polyclonal anti-mCherry	Abcam	Cat#ab167453
Rabbit polyclonal anti-MAP2	Synaptic Systems	Cat#188002
Mouse monoclonal anti-Ankyrin G	Santa Cruz	Cat#sc-12719
Rabbit polyclonal anti-βIV-Spectrin	ThermoFisher	Cat#PA5-62972
Guinea pig polyclonal anti-VGAT	Synaptic Systems	Cat#131004
Guinea pig polyclonal anti-Synapsin I	Synaptic Systems	Cat#106104
Mouse monoclonal anti-βIII-tubulin	Sigma	Cat#T8660
Rabbit polyclonal anti-GAPDH	Abcam	Cat#ab9485
Goat anti-mouse Alexa 405	ThermoFisher	Cat#A31553
Donkey anti-rat Alexa 488	ThermoFisher	Cat#A21208
Goat anti-chicken Alexa 488	ThermoFisher	Cat#A11039
Goat anti-rabbit Alexa 555	ThermoFisher	Cat#A21428
Goat anti-rat Alexa 568	ThermoFisher	Cat#A11077
Goat anti-rabbit Alexa 568	ThermoFisher	Cat#A11036
Goat anti-guinea pig Alexa 594	ThermoFisher	Cat#A11076
Goat anti-rat Alexa 594	Jackson ImmunoResearch	Cat#112-585-167
Donkey anti-rabbit Alexa 647	ThermoFisher	Cat#A31573
Donkey anti-mouse Alexa 647	Jackson ImmunoResearch	Cat#715-605-150
Goat anti-mouse Alexa 647	Jackson ImmunoResearch	Cat#115-605-166
Donkey anti-guinea pig Alexa 647	Jackson ImmunoResearch	Cat#706-605-148
Goat anti-mouse Atto 647N	Sigma	Cat#50185
Goat anti-rat IRDye 800CW	LI-COR	Cat#925-32219
Goat anti-rabbit IRDye 800CW	LI-COR	Cat#926-32211
Goat anti-rabbit IRDye 680RD	LI-COR	Cat#926-68071
Bacterial and Virus Strains		
E. coli NEB Stable	NEB	Cat#C3040
E. coli One Shot Stbl3	ThermoFisher	Cat#C737303
AAV2/1 encapsulated HiUGE vectors	This paper	N/A
AAV2/9 encapsulated HiUGE vectors	This paper	N/A
AAV2-retro encapsulated HiUGE vectors	This paper	N/A
Chemicals, Peptides, and Recombinant Proteins		
D-AP5	Tocris	Cat#0106
Cytosine arabinoside	Sigma	Cat#C1768
Polyethylenimine (PEI)	Polysciences	Cat#24765
Benzonase	Novagen	Cat#70664
Lipofectamine 3000	ThermoFisher	Cat#L3000008

(*Continued on next page*)

Continued

REAGENT or RESOURCE	SOURCE	IDENTIFIER
Normal goat serum	Sigma	Cat#G9023
Optiprep density gradient	Sigma	Cat#D1556
Critical Commercial Assays		
BCA protein assay	Pierce	Cat#23227
InFusion cloning kit	TaKaRa	Cat#638910
TOPO TA Cloning Kit for Sequencing	ThermoFisher	Cat#K457501
CanGetSignal solution	TOYOBO	Cat#NKB-101T
MyTaq Extraction-PCR kit	Bioline	Cat#BIO-21127
PureLink Genomic DNA Mini Kit	ThermoFisher	Cat#K182001
DNeasy Blood & Tissue Kit	QIAGEN	Cat#69504
MyTaq HS Mix	Bioline	Cat#BIO-25045
MyTaq HS Red Mix	Bioline	Cat#BIO-25047
PowerUp SYBR Green Master Mix	ThermoFisher	Cat#A25741
SensiFAST Real-Time PCR Kit	Bioline	Cat#BIO-86005
Genome Walker kit	Clontech	Cat#636406
Amicon Ultra-15 filtration unit	Millipore	Cat#UFC910008
Spin-X centrifuge tube filter	Costar	Cat#8162
Experimental Models: Cell Lines		
HEK293T cells	ATCC	CRL-11268
NIH 3T3 cells	ATCC	CRL-1658
HeLa cells	ATCC	CCL-2
Experimental Models: Organisms/Strains		
Mouse: $\text{Gt(ROSA)26Sor}^{\text{tm1(CAG-cas9*,-EGFP)Fezh}}$	Jackson Laboratory	024857
Mouse: C57BL/6J	Jackson Laboratory	000664
Oligonucleotides		
Donor Recognition Sequences (DRS), see Table S1	This paper	N/A
Guide RNA (gRNA) targets, see Table S1	This paper	N/A
Donor sequences, see Table S1	This paper	N/A
Primers, see Table S1	This paper	N/A
Recombinant DNA		
AAV:ITR-U6-sgRNA(backbone)-hSyn-Cre-2A-EGFP-KASH-WPRE-shortPA-ITR	Feng Zhang (Platt et al., 2014)	Addgene Plasmid #60231
pAAV-nEFCas9	Juan Belmonte (Suzuki et al., 2016)	Addgene Plasmid #87115
rAAV2-retro helper	Alla Karpova & David Schaffer (Tervo et al., 2016)	Addgene Plasmid #81070
pCAG-smFP HA	Loren Looger (Viswanathan et al., 2015)	Addgene Plasmid #59759
pAAV-HiUGE-GS-gRNA vectors	This paper	N/A
pAAV-HiUGE-Donor vectors	This paper	N/A
pAAV-HiUGE-GS-gRNA vectors with intein-split-Cas9	This paper	N/A
pAAV-HiUGE-Donor vectors with intein-split-Cas9	This paper	N/A
Software and Algorithms		
FIJI	Schindelin et al., 2012; Schneider et al., 2012	https://fiji.sc
CRISPOR	Haeussler et al., 2016	http://crispor.tefor.net
Cas-OFFinder	Bae et al., 2014	http://www.rgenome.net/cas-offinder
Trim Galore Toolkit (v 0.5.0)	Babraham Bioinformatics	http://www.bioinformatics.babraham.ac.uk/projects/trim_galore

(*Continued on next page*)

Continued

REAGENT or RESOURCE	SOURCE	IDENTIFIER
Trimmomatic	Bolger et al., 2014	http://www.usadellab.org/cms/?page=trimmomatic
Cutadapt (v 1.18)	Martin, 2011	https://pypi.org/project/cutadapt/
FastQC (v 0.11.5 or v 0.11.8)	Babraham Bioinformatics	https://www.bioinformatics.babraham.ac.uk/projects/fastqc
bwa-mem (v0.7.17)	Li and Durbin, 2009	https://sourceforge.net/projects/bio-bwa/files/
SAMtools (v1.9)	Li et al., 2009	https://github.com/samtools/samtools
Picard	Broad Institute	http://broadinstitute.github.io/picard
GATK HaplotypeCaller (v3.8-1-0-gf15c1c3ef)	McKenna et al., 2010	https://software.broadinstitute.org/gatk/
FLASH	Magoč and Salzberg, 2011	https://ccb.jhu.edu/software/FLASH/
EMBOSS Needle	Chojnacki et al., 2017	https://www.ebi.ac.uk/Tools/psa/emboss_needle/nucleotide.html
CRISPResso	Pinello et al., 2016	http://crispresso.rocks/
R	The R Foundation	https://www.r-project.org/
JMP Pro	SAS	https://www.jmp.com
Other		
Zeiss LSM 880	Zeiss	N/A
Zeiss LSM 710	Zeiss	N/A
Zeiss Imager.M2 with Apotome.2	Zeiss	N/A
Leica STED microscope	Leica	N/A
Odyssey Fc Imager	LI-COR	N/A

LEAD CONTACT AND MATERIALS AVAILABILITY

Further information and requests for resources and reagents should be directed to and will be fulfilled by the Lead Contact, Dr. Scott Soderling (scott.soderling@duke.edu).

EXPERIMENTAL MODEL AND SUBJECT DETAILS

Gt(ROSA)26Sor$^{tm1(CAG-cas9\star,-EGFP)Fezh}$ (Cas9) and C57BL/6J mice

For *in vivo* studies, Gt(ROSA)26Sor$^{tm1(CAG-cas9\star,-EGFP)Fezh}$ mice (Cas9 mice, Jackson Laboratory) or wild-type (WT) C57BL/6J mice (Jackson Laboratory) were used. For intracranial injections, neonatal pups (P0-P2, undetermined sex) were used. Sex determination at this development stage is both visually difficult and unnecessary for the experiment. For stereotaxic local injections, adult male mice (> 8 weeks of age) were used. Mice were group-housed in the Duke University's Division of Laboratory Animal Resources facility. All procedures were performed with a protocol approved by the Duke University Institutional Animal Care and Use Committee in accordance with US National Institutes of Health guidelines.

Primary mouse hippocampal and cortical neuron / glia culture

Primary neuron / glia cultures were derived from Gt(ROSA)26Sor$^{tm1(CAG-cas9\star,-EGFP)Fezh}$ or C57BL/6J (Jackson Laboratory) neonatal pups (P0-P2). Primary culture was performed following a previously described method (Uezu et al., 2016). Briefly, after euthanasia, brains were rapidly collected, and hippocampi or cortices were isolated. Cells were gently dissociated with fire polished glass pipettes following papain digestion (Worthington), and plated at a density of ~100,000 cells per cm^2 (for imaging, hippocampal cells), or ~300,000 cells per cm^2 (for DNA / protein preparation, cortical cells) on poly-L-lysine (Sigma P2636) coated surfaces. Cells were then maintained in Neurobasal A medium (ThermoFisher 10888022) supplemented with 2% B27 (ThermoFisher 17504044) and 1% GlutaMAX (ThermoFisher 35050061) at 37°C, 5% CO_2. Glia growth was inhibited by adding cytosine arabinoside (Sigma C1768, 5uM final concentration) together with media change between DIV 4-6, when necessary.

Cell culture of HEK293T, HeLa, and NIH 3T3 cell lines

Cell lines used in this study include HEK293T (ATCC CRL-11268), HeLa (ATCC CCL-2), and NIH 3T3 (ATCC CRL-1658). All cell lines were maintained in DMEM (GIBCO 11965-092) supplemented with 10% fetal bovine serum (Sigma F4135) and 1% Penicillin-Streptomycin (ThermoFisher 15140122) at 37°C, 5% CO_2, and passaged by trypsin/EDTA digestion (ThermoFisher 25200056) upon reaching ~95% confluency.

METHOD DETAILS

Construction of HiUGE Vectors

Both the gene-specific vector and the HiUGE donor vector were derived from a backbone vector AAV:ITR-U6-sgRNA-hSyn-Cre-2A-EGFP-KASH-WPRE-shortPA-ITR (a gift from Feng Zhang (Platt et al., 2014), Addgene plasmid # 60231).

Gene-specific gRNA (GS-gRNA) vector backbone were prepared by removing the HA-2A-EGFP-KASH fragment from the backbone plasmid. These vectors express GS-gRNAs driven by a U6 promoter, as well as Cre-recombinase driven by a neuronal specific hSyn promoter. For gRNA targeting non-neuronal cells (glia, etc.), the hSyn promoter was swapped with the ubiquitous Ef1α promoter to drive Cre expression. These vectors were used in conjunction with Gt(ROSA)26Sor$^{tm1(CAG-cas9*,-EGFP)Fezh}$ mice (Cas9 mice) for Cre-dependent Cas9 expression. For each gene of interest (GOI), GS-gRNA sequences targeting either the N-term or the C-term of the GOI were designed using an online gRNA evaluation tool "CRISPOR" (Haeussler et al., 2016), and cloned into the SapI site using a highly efficient (typically > 90% positive rate of colony picking, Figures S1F–S1H) restriction digestion / ligation cloning method. In brief, 10ng (~2fmol) of the GS-gRNA backbone plasmid was digested with SapI enzyme (NEB R0569, 1uL) and simultaneously ligated with 50fmol of annealed 23-24-mer (including SapI sticky ends) GS-gRNA oligos with T4 DNA ligase (NEB M0202, 1uL) in a 10uL reaction, by 10 repeats of thermocycling between 37°C (5 min) and 21°C (5 min). Colony PCR was performed to detect GS-gRNA integration into the backbone plasmid using a forward primer in the upstream U6 promoter region, paired with the reverse GS-gRNA oligo as the reverse primer to amplify an ~100bp amplicon. GS-gRNA target sequences used in this study were listed in Table S1.

For HiUGE donor vectors, a donor-specific gRNA (DS-gRNA) was cloned into the SapI site behind the U6 promoter. The fragment between the XbaI and PmlI restriction sites was replaced with payload sequences to be inserted to the targeted genomic loci, such as epitope tags (HA, Myc, and V5), fluorescent proteins (Shaner et al., 2004; Zacharias et al., 2002), "spaghetti monster" fluorescent protein-HA (a gift from Loren Looger (Viswanathan et al., 2015), Addgene plasmid # 59759), and cellular trafficking tag (SV40 nuclear localization signal, NLS). The payload sequences were flanked on both ends by a donor recognition sequence (DRS), that is an artificial sequence not present in the human or mouse genome and is specifically recognized by the DS-gRNA with low genomic off-target liability (exemplary DS-gRNA has a CRISPOR specificity score of 98 or higher against human or mouse genome, with no genomic targets within 3-basepair mismatches), as predicted by CRISPOR and Cas-OFFinder (Bae et al., 2014; Haeussler et al., 2016; Hsu et al., 2013). The DS-gRNA directs Cas9-mediated DRS cleavage and release of the payload sequence to be inserted into the targeted genomic locus. Exemplary DRS and payload sequences used in this study can be found in Table S1.

In addition, to facilitate genome editing in wild-type cells and animals without extra source of Cas9 expression, an intein-split-Cas9 system (Truong et al., 2015) was used to distribute Cas9 coding sequences to both the GS-gRNA vector and the HiUGE donor vector. In this case, the GS-gRNA vectors were constructed by replacing hSyn-Cre with the EF1α/HTLV (nEF) promoter (nEF-Cas9, a gift from Juan Belmonte (Suzuki et al., 2016), Addgene plasmid # 87115) followed by C-intein-C-Cas9 coding sequences between XbaI and PmlI sites. The donor vectors were constructed by the addition of N-Cas9-N-intein coding sequences, also driven by the nEF promoter, behind the payload sequences of the donor vectors.

AAV Production

Purified AAV was produced following a previously described method (Uezu et al., 2016). Briefly, HEK293T cells were plated on six 15cm dishes and transfected with 15μg HiUGE AAV vector (either GS-gRNA or donor payload), 30μg helper plasmid pAd-DeltaF6, and 15μg AAV serotype 2/9 plasmid per six dishes with PEI Max (Polysciences 24765) when reaching 60%–80% confluency. Cells were then incubated in DMEM with glutamine and pyruvate (Corning 10-013-CV), supplemented with 10% FBS (Sigma F4135). Cells were harvested 3 days after transfection and lysed with 3 repeats of freeze-thaw cycles, followed by treatment with Benzonase (Novagen 70664) at 37°C for 30 minutes. Cell lysate was then applied to an Optiprep density gradient (Sigma D1556, 15%, 25%, 40% and 60%) for ultracentrifugation purification. AAV-enriched fraction was collected, then further concentrated by repeated washes with sterile PBS in an Amicon Ultra-15 filtration unit (NMWL: 100kDa, Millipore UFC910008) to a final volume of ~100 μL and aliquoted for storage at −80°C. For preparing AAV2-retro, 15μg rAAV2-retro plasmid (a gift from Alla Karpova & David Schaffer (Tervo et al., 2016), Addgene plasmid # 81070) was used as the serotype plasmid. Similar transfection and viral purification procedure described above was used. Real-time PCR reactions were performed with PowerUp SYBR Green Master Mix (Thermo A25741) using primers targeting the ITR of AAV2 to measure viral titers against copy number standards (Aurnhammer et al., 2012). Primer sequences are listed in Table S1. Titers of purified AAVs used in this study were: *Sptbn4* C-term GS-gRNA (AAV2/9 serotype. Batch 1: 4.7 × 10^{11} GC / μL, Figure 3B; Batch 2: 2.9 × 10^{11} GC / μL, Figures S3A–S3C; Batch 3: 3.9 × 10^{11} GC / μL, Figures 3F–3J and S4A–S4C; Batch 4: 1.8 × 10^{11} GC / μL, Figures S2D–S2F); *Scn2a* C-term GS-gRNA (AAV2/9 serotype. Batch 1: 4.7 × 10^{11} GC / μL, Figures 3C and S3F–S3H; Batch 2: 9.7 × 10^{11} GC / μL, Figures S3A–S3E; Batch 3: 3.6 × 10^{11} GC / μL, Figures 3F–3J, S2A–S2C, S2G–S2I, S4A, and S4B; Batch 4: 9.6 × 10^{10} GC / μL, Figures S2G–S2I); *Tubb3* C-term GS-gRNA (AAV2/9 serotype. Batch 1: 6.7 × 10^{11} GC / μL, Figures 3D, 4C, and 4D; Batch 2: 2.7 × 10^{11} GC / μL, Figures S1B and S1C); *Mecp2* C-term GS-gRNA (AAV2/9 serotype. 6.4 × 10^{11} GC / μL, Figure 3E); *Map2* C-term GS-gRNA (AAV2/9 serotype. 4.4 × 10^{11} GC / μL, Figures S3A–S3C); *Actr2* C-term GS-gRNA (AAV2/9 serotype. 1.3 × 10^{11} GC / μL, Figures S3A–S3C); *Clta* C-term GS-gRNA (AAV2/9 serotype. 2.3 × 10^{11} GC / μL, Figures S3A–S3C); empty GS-gRNA (AAV2/9 serotype. Batch 1: 9.1 × 10^{11} GC / μL, Figures S1B and S1C; Batch 2: 2.7 × 10^{11} GC / μL, Figures S2D–S2I); HA-epitope donor (AAV2/9 serotype, ORF+1. Batch 1: 1.4 × 10^{11} GC / μL, Figures 3A–3E, 4C, 4D, and S3F–S3H; Batch

2: 1.1 × 10^{11} GC / μL, Figures 5, S1B, and S1C; Batch 3: 1.8 × 10^{10} GC / μL, Figures S3A–S3E; Batch 4: 3.8 × 10^{10} GC / μL, Figures S3A–S3C; Batch 5: 1.4 × 10^{11} GC / μL, Figures S4A–S4C; Batch 6: 3.4 × 10^{10} GC / μL, Figures 3F–3J and S2A–S2C; Batch 7: 1.2 × 10^{10} GC / μL, Figures S2D–S2I; Batch 8: 2.2 × 10^{10} GC / μL, Figures S2D–S2I); HA-epitope donor (AAV2/9 serotype, ORF+0. 1.3 × 10^{10} GC / μL, Figures S1B and S1C); HA-epitope donor (AAV2/9 serotype, ORF+2. 5.9 × 10^{10} GC / μL, Figures S1B and S1C); HA-epitope donor (AAV2/9 serotype, ORF+1 with DRS-2. 2.2 × 10^{10} GC / μL, Figures S2A–S2C); HA-epitope donor (AAV2/9 serotype, ORF+1 with DRS-3. 1.6 × 10^{10} GC / μL, Figures S2A–S2C); Myc-epitope donor (AAV2/9 serotype, ORF+1. 2.4 × 10^{11} GC / μL, Figures 4C–4D and 5A–5H); *Tubb3* C-term GS-gRNA (AAV2-retro serotype. 2.7 × 10^{9} GC / μL, Figure 5); *Map2* C-term GS-gRNA with intein-split-Cas9 (AAV2/9 serotype. 7.6 × 10^{10} GC / μL, Figures 7Oand 7P); *Sptbn4* C-term GS-gRNA with intein-split-Cas9 (AAV2/9 serotype. 8.5 × 10^{10} GC / μL, Figures S5B–S5D); HA-epitope donor with intein-split-Cas9 (AAV2/9 serotype, ORF+1. Batch 1: 3.0 × 10^{10} GC / μL, Figures 7O and 7P, Batch 2: 2.2 × 10^{11} GC / μL, Figures S5B–S5D); *Sptbn4*-HITI HA-epitope donor (AAV2/9 serotype, 1.6 × 10^{11} GC / μL, Figures S2D–S2F); *Scn2a*-HITI HA-epitope donor (AAV2/9 serotype, 8.1 × 10^{10} GC / μL, Figures S2G–S2I). For quantitative experiments, AAVs were added to primary cultures at a final concentration of 5 × 10^{10} GC / mL per virus in the culture medium, unless otherwise stated.

For small-scale AAV supernatant, HEK293T cells were plated on a 12 well plate, then transfected with 0.4μg AAV plasmid, 0.8μg helper plasmid pAd-DeltaF6, and 0.4μg serotype 2/1 plasmid per well with PEI Max (Polysciences 24765) when cell density reached 60%–80% confluency. Cells were then incubated in glutamine-free DMEM (ThermoFisher 11960044) supplemented with 1% Glutamax (ThermoFisher 35050061) and 10% FBS (Sigma F4135) for 3 days. The AAV-containing supernatant medium was collected and filtered through a 0.45 μm cellulose acetate Spin-X centrifuge tube filter (Costar 8162), and temporarily stored at 4°C for no more than 2 weeks. Titers of small-scale AAVs were typically 10^{8} - 10^{9} GC / μL.

Stereotaxic Injections

For stereotaxic injections, adult mice were anesthetized through inhalation of 1.5% isofluorane gas and placed in a stereotaxic frame (Kopf Instruments). Mice were administered meloxicam (~10 μL / 25 g) subcutaneously before the beginning of surgery to reduce inflammation. After confirming that Lambda and Bregma were on the same dorsal-ventral plane, craniotomies were made with a high speed drill (Foredom MH-170) over either motor cortex (0.5 A/P, 0.6-1.0 L, 1.2 V), striatum (0.5 A/P, 2.0 L, 3.2 V), thalamus (−1.7 A/P, 1.2 L, 3.4 V), posterior somatosensory cortex (−1.7 A/P, 3.5 L, 1.2 V), or dorsal hippocampus (−1.6 A/P, 2.2 L, 1.3 V), in reference to the Allen Mouse Brain Atlas (Lein et al., 2007). Using a precision pressure injection system (Drummond Nanoject), a glass pipette filled with virus was lowered to the desired depth, slightly retracted (~0.2mm), and small amounts of virus were injected over a period of ~10 minutes (30 injections of 18-32 nL every 20 s). After waiting for an additional 5-10 minutes to prevent efflux of virus during pipette retraction, the glass pipette was retracted from the brain and the skin over the craniotomy was sutured shut. After applying several drops of topical anesthetic to the incision (bupivacaine) and administering an analgesic subcutaneously (buprenorphine, ~25 μL / 25 g), mice were allowed to recover under a heat lamp for 20-30 minutes and then placed in their home cage.

In Vitro and *In Vivo* Protein Modification by HiUGE

For *in vitro* qualitative experiments, primary cultures were prepared using neonatal pups (P0-P2) of Gt(ROSA)26Sor$^{tm1(CAG-cas9*,-EGFP)}$ ^{Fezh} mice (Cas9 mice), and transduced with combinations of small-scale AAV supernatants (GS-gRNA and donor payload). The filtered supernatants were added directly to primary cultures together with media change on DIV 4-6 for transduction (100-200 μL per well on a 24 well plate). NMDA receptor antagonist D-APV (Tocris 0106, ~50μM final concentration) was added to protect neurons against toxicity associated with media change (Hogins et al., 2011). Alternatively, combinations of small-scale AAV supernatants were added to primary cultures at DIV 1 (in this case D-APV is not necessary); and incubated together with the neurons until the day of fixation to extend the accumulation period of the nascently modified proteins. For quantitative *in vitro* experiments, purified AAVs were added to primary cultures with the final concentration of 5 × 10^{10} GC / mL per virus in the culture medium, unless otherwise stated. On the day of fixation (DIV 11-14), cells were treated with 4% PFA + 4% sucrose in PBS for 15 minutes at 4°C and used for immunocytochemistry to detect HiUGE-mediated KI. For qualitative *in vivo* applications, purified high-titer AAVs were combined (GS-gRNA and donor payload, 1:1 v/v) and intracranially injected (~2μL per hemisphere) to neonatal pups of Cas9 mice (P0-P2). For quantitative *in vivo* experiments, purified AAVs were combined with a final titer of 3 × 10^{10} GC/μL for each virus, and locally injected to the motor cortex of adult Cas9 mice. For neural circuit-selective applications, adult Cas9 mice received a stereotaxic injection of purified AAV2-retro GS-gRNA virus into the brain area containing axon terminals of a specific neural circuit, whereas separate injections of purified AAV2/9 HiUGE donor virus were delivered into the brain area containing projection neuron cell bodies. 2-3 weeks after injection, mice were euthanized, and brains were isolated either fresh frozen with dry ice, or after transcardial perfusion, for immunohistochemistry to detect HiUGE-mediated KI.

For HiUGE vectors that have built-in intein-split-Cas9 expression, primary culture derived from WT C57BL/6J mice (P0-P2) or other common cell lines (HeLa, HEK293T, NIH 3T3) were used. Small-scale AAVs were used to transduce primary neurons as described above in similar applications. Further, to demonstrate that these HiUGE components were also suitable to be delivered via plasmid transfection rather than AAV transduction in common cell lines of human or mouse origin, HiUGE GS-gRNA and donor plasmids were co-transfected into HeLa, HEK293T, or NIH 3T3 cells with PEI MAX (Polysciences 24765) or Lipofectamine 3000 (ThermoFisher L3000008) following manufacturer's protocol. Cells were fixed 2-4 days after transfection for immunocytochemistry to detect

HiUGE-mediated KI. For *in vivo* testing, purified high-titer AAVs (GS-gRNA and donor payload) were combined, then stereotaxically injected to specific brain areas of adult WT mice. 2-3 weeks after injection, mice were euthanized, and transcardially perfused. Brains were isolated for immunohistochemistry to detect HiUGE-mediated KI.

Immunohistochemistry and Immunocytochemistry

For immunohistochemistry (IHC), both fresh frozen specimens and perfused specimens were used. For fresh frozen specimens (when working with AIS proteins), the animal was euthanized, and its brain was quickly isolated, frozen on crushed dry ice, coronally sectioned at 20μm thickness and mounted on glass slides (VWR). The specimen was fixed with 4% PFA + 4% sucrose in PBS for 15 minutes at 4°C. IHC was then performed. The specimen was blocked and permeabilized with blocking buffer containing 0.3% Triton-X, 5% normal goat serum (NGS, Sigma) in PBS for 30-60 min at room temperature, and primary antibodies were applied for 2 hr at room temperature or at 4°C overnight. Fluorescent secondary antibodies were applied for 30-60 min at room temperature, and counterstained with DAPI. For perfused specimens (when working with non-AIS proteins), the animal was euthanized and transcardially perfused with ice cold heparinized (25U / mL) PBS, followed by 4% PFA in PBS. Brains were harvested and post-fixed in 4% PFA overnight at 4°C and cryoprotected in 30% sucrose + 10% glycerol in PBS at 4°C. Brains were coronally sectioned at 40-80μm thickness for free-float antibody incubation. Similar IHC incubation conditions as described above were used for free-float sections 50μm or thinner. For thicker sections (> 50μm), incubation durations were doubled to allow sufficient penetration of antibody. The specimens were then mounted to glass slides and coverslipped with FluorSave reagent (Millipore 345789).

For immunocytochemistry (ICC), cells grown on glass coverslips were fixed with 4% PFA + 4% sucrose in PBS for 15 minutes at 4°C, then blocked and permeabilized with blocking buffer containing 0.3% Triton-X, 5% NGS in PBS for 30-60 min at room temperature. Primary antibodies were applied for 2 hr at room temperature or at 4°C overnight. Fluorescent secondary antibodies were applied for 30-60 min at room temperature, and counterstained with DAPI. The coverslips were then mounted to glass slides with FluorSave reagent (Millipore 345789).

Primary antibodies used for IHC/ICC were listed as following with dilutions indicated in parentheses: rat anti-HA (Roche/Sigma 11867423001, 1:1000), mouse anti-HA (BioLegend MMS-101P, 1:250), rabbit anti-Myc (Santa Cruz sc-789, 1:250), mouse anti-V5 (ThermoFisher R960-25, 1:500), chicken anti-GFP (Abcam ab13970, 1:2000), rabbit anti-mCherry (Abcam ab167453, 1:1000), rabbit anti-MAP2 (Synaptic Systems 188002, 1:5000), mouse anti-Ankyrin G (Santa Cruz sc-12719, 1:250), rabbit anti-βIV-spectrin (ThermoFisher PA5-62972, 1:1000), guinea pig anti-VGAT (Synaptic Systems 131004, 1:2000), guinea pig anti-Synapsin I (Synaptic Systems 106104, 1:250), mouse anti-βIII-tubulin (Sigma T8660, 1:1000). Fluorophore-conjugated secondary antibodies or reagents used for IHC/ICC were listed as following: goat anti-mouse Alexa 405 (ThermoFisher A31553 1:1000), donkey anti-rat Alexa 488 (ThermoFisher A21208, 1:1000), goat anti-chicken Alexa 488 (ThermoFisher A11039 1:1000), goat anti-rabbit Alexa 555 (ThermoFisher A21428, 1:1000), goat anti-rat Alexa 568 (ThermoFisher A11077 1:1000), goat anti-rabbit Alexa 568 (ThermoFisher A11036, 1:1000), goat anti-guinea pig Alexa 594 (ThermoFisher A11076, 1:100 for STED), goat anti-rat Alexa 594 (Jackson ImmunoResearch 112-585-167, 1:1000), donkey anti-rabbit Alexa 647 (ThermoFisher A31573, 1:1000), donkey anti-mouse Alexa 647 (Jackson ImmunoResearch 715-605-150, 1:1000), goat anti-mouse Alexa 647 (Jackson ImmunoResearch 115-605-166, 1:1000), donkey anti-guinea pig Alexa 647 (Jackson ImmunoResearch 706-605-148, 1:1000), goat anti-mouse Atto 647N (Sigma 50185, 1:100 for STED).

Microscopic Fluorescence Imaging

Microscopic images were acquired with Zeiss 710 or Zeiss 880 inverted confocal microscopes, or with Zeiss Imager.M2 upright microscope equipped with an Apotome module. Stimulated emission depletion (STED) images were acquired on a Leica STED system. Exposures were manually adjusted for optimal dynamic range. Tiling and z stack were performed when necessary. Tiled images were stitched in Zeiss Zen for composite presentation (Figures 3, 4, 5, and 7). Brightness, contrast, and gamma correction were adjusted for each channel using Zeiss Zen or FIJI (Schindelin et al., 2012; Schneider et al., 2012). When comparisons against control conditions were necessary, identical exposure and adjustment parameters were used across the cohort. Live imaging was performed on Zeiss 710 microscope at 37°C, with 5% CO_2 incubation. Time series of z stacked images were acquired every 100 s, then processed and exported at 6 fps in FIJI as videoclip followed by annotation in Adobe After Effects. All images were pseudocolored for presentation with color assignments indicated in each panel.

Western Blot

Cells were collected in ice cold RIPA buffer supplemented with proteinase inhibitor cocktail and sonicated. Protein concentrations were determined by BCA method and equal amounts of protein were heated in sample buffer at 95°C for 5 min, loaded for SDS/PAGE electrophoresis, then transferred to a nitrocellulose membrane. Following blocking in blocking buffer (Rockland MB-070), the membrane was sequentially probed for HA-epitope (primary: rat anti-HA, Roche/Sigma 11867423001, 1:2000; secondary: IRDye 800CW goat anti-rat, 1:10,000) and house-keeping gene GAPDH (primary: rabbit anti-GAPDH, Abcam ab9485, 1:5000; secondary: IRDye 680RD goat anti-rabbit, 1:10,000). Both primary and secondary antibodies were incubated for 1hr at room temperature. Immunofluorescence signal was detected on Odyssey FC imager (LI-COR). For immunoprecipitation (IP)-enriched western blot to detect the serial truncation of βIV-spectrin, equal amount of inputs (300μg) were mixed with 30μL mouse anti-HA beads (ThermoFisher 26181) and incubated at 4°C overnight on a nutator. After washes with RIPA buffer, proteins were eluted by boiling in 80μL sample buffer at 95°C for 5 min. Equal volume of the eluted IP-samples and equal amount of the input samples were loaded for SDS/PAGE and then transferred to nitrocellulose membranes. The IP-membrane was sequentially probed for HA-epitope (primary: Sigma H6908, 1:2000; secondary: IRDye 800CW goat anti-rabbit, 1:10,000) and the input membrane was probed for house-keeping gene GAPDH (primary: Abcam ab9485, 1:5000; secondary: IRDye 680RD goat anti-rabbit, 1:10,000). Both primary and secondary antibodies were incubated for 1 hr at room temperature in CanGetSignal solutions (TOYOBO NKB-101T). Immunofluorescence signal was detected and processed on an Odyssey FC imager (LI-COR).

Genomic PCR, TOPO Cloning and DNA Sequencing

Genomic DNA was extracted by MyTaq Extraction-PCR kit (Bioline BIO-21127) or PureLink Genomic DNA Mini Kit (ThermoFisher K182001) from primary neurons after HiUGE editing. Genomic polymerase chain reaction (PCR) using MyTaq HS polymerase (Bioline BIO-25045 or BIO-25047) was performed to detect the insertion of the dual-orientation HA-epitope payload using primers indicated in Table S1. A primer specific for the endogenous genomic sequence upstream of the edited locus was paired with an orientation-selective HA-epitope payload primer to amplify the edited genomic locus and differentiate forward versus reverse payload integration. PCR products were isolated by gel purification (NucleoSpin Gel and PCR Clean-up kit, Macherey Nagel 740609) and TOPO-cloned (ThermoFisher K457501) for sequencing using a common M13F(−21) primer (Eton Bioscience). For indel estimation, genomic DNA were extracted from triplicate neuronal samples following HiUGE-mediated HA-epitope KI. Genomic PCRs were performed using primer pairs that were either insert-specific (described above), or across the edited junction. The PCR products were cleaned up (NucleoSpin Gel and PCR Clean-up kit, Macherey Nagel 740609), combined into three independent pools, and deep sequenced on a MiSeq system (Illumina) by the Duke Sequencing and Genomic Technologies Shared Resource.

Assessment of genomic off-target integration

The GS-gRNA targeting mouse *Scn2a*, which has a mediocre CRISPOR specificity score of 66 out of 100 (best), was used as an example to assess the off-target effects of HiUGE-mediated genome editing. First, genomic primers surrounding the top CRISPOR predicted off-target loci (3 for DS-gRNA, 5 for *Scn2a* GS-gRNA) were designed using NCBI Primer-BLAST (Ye et al., 2012) (sequences listed in Table S1). Genomic DNA was prepared from HiUGE-edited primary neurons incubated with a combination of *Scn2a* GS-gRNA and HA-epitope donor, using PureLink Genomic DNA Mini Kit (ThermoFisher K182001). PCR reactions were performed by pairing the genomic primer with the insert-specific primer to detect genomic integration of the HA-epitope payload in either forward or reverse orientation. Meanwhile, PCR using pairs of forward and reverse genomic primers spanning the off-target loci were performed as controls. PCR products were electrophoresed on agarose gel and imaged under UV light. Further, genome-wide identification of potential off-target integration of the payload was performed using Genome Walker kit (Clontech 636406). Genomic DNA was prepared from *in vivo* edited mouse brain injected with a combination of *Scn2a* GS-gRNA and HA-epitope donor, using DNeasy Blood & Tissue Kit (QIAGEN 69504). Restriction enzyme digestion, adaptor ligation and nested PCR was performed according to the manufacturer's protocol (primer sequences listed in Table S1), followed by band purification and sequencing. Three potential genomic off-target integrations of the payload were identified. Primers surrounding these sites were designed (sequences listed in Tables S1). PCR reactions were performed by pairing the genomic primer with the insert-specific primer to detect genomic integration of the HA-epitope payload in either forward or reverse orientation. In addition, real-time PCR was performed in duplicates using SensiFAST Real-Time PCR Kit (Bioline BIO-86005).

QUANTIFICATION AND STATISTICAL ANALYSIS

For immunofluorescence quantification of C-term HA-epitope KI to mouse *Tubb3*, microscopic images were taken by an experimenter blinded to the experimental groups, using identical exposure parameters across the cohort. Three coverslips were used per experimental group, with three microscopic images taken per coverslip at random locations. The HA immunofluorescence intensity of an image was quantified by FIJI after automatic background subtraction. The total cell count of an image was estimated by particle analysis of DAPI fluorescence in FIJI. A ratio of mean HA immunoreactivity over cell count was computed, then normalized on a scale of 0-100 arbitrary unit (a.u.), against the negative group (no virus added) and the positive group (*Tubb3* GS-gRNA plus HiUGE donor ORF+1). The normalized ratio was defined as the "mean fluorescence intensity." Also, cells positive for HA immunoreactivity were tallied and their percentages over total cell counts were calculated. The quantification results were averaged for each coverslip and reported (n = 3). For immunofluorescence quantification of C-term HA-epitope KI to AIS protein targets *in vitro*, microscopic images were taken by an experimenter blinded to the experimental groups, using identical exposure parameter across the cohort. Three coverslips were used per experimental group, with three microscopic images taken per coverslip at random locations. The number of AIS structures positive for HA-epitope immunofluorescence and the total number of Ank-G-positive AIS were manually counted by a blinded experimenter, then converted into percentages for analysis. The quantification results were averaged for each coverslip and reported (n = 3). For quantification of HiUGE labeling efficiency *in vivo*, three adult Cas9 mice were stereotaxically injected with HiUGE AAVs into the motor cortex per group and analyzed by immunohistochemistry 2 weeks following injection. Four microscopic images were taken for each mouse at the injection site from separate coronal sections. The number of AIS structures positive for HA-epitope immunofluorescence and the total number of βIV-Spectrin-positive AIS structures were manually counted by a blinded experimenter, then converted into percentages for analysis. The quantification results were averaged for each mouse and reported (n = 3). For the comparison experiment with HITI, the Cre-expressing empty GS-gRNA AAV was used to induce Cas9 expression in primary neuronal cultures from Cas9 mice, together with the HA-epitope HITI donor vectors to facilitate genome editing. Two targets (mouse *Sptbn4* and *Scn2a*) were edited by either HiUGE or HITI with 7 coverslips used for each group. Three microscopic images were taken per coverslip at random locations by a blinded experimenter. The number of AIS structures positive for HA-epitope immunofluorescence and the total number of Ank-G-positive AIS were manually counted by a blinded experimenter, converted into percentages, averaged for each coverslip, and normalized to the HITI group of each gene to assess the comparative efficiencies between the two methods (n = 7). To detect pairwise differences, two-tailed t test or one-way ANOVA followed by post hoc Tukey-Kramer HSD test was performed in JMP Pro (v13, SAS), with significance level set at 0.05.

For quantitative estimation of the indel rate at the edited junctions upstream of the payload, raw single-end read sequences of the insert-specific PCR products were trimmed of adaptor and poor-quality sequences using the Trim Galore Toolkit (v 0.5.0, http://www.bioinformatics.babraham.ac.uk/projects/trim_galore), which employs Cutadapt (Martin, 2011) (v 1.18). The quality of the raw reads was verified by examining the FastQC (v 0.11.5, https://www.bioinformatics.babraham.ac.uk/projects/fastqc) output from Trim Galore. A reference FASTA file containing the amplicon sequence for each of the genes by integration (forward and reverse) combinations was prepared, which included ten sequences in total. Quality-trimmed reads were aligned to the reference FASTA file with bwa-mem (Li and Durbin, 2009) (v0.7.17) with default parameters and post-processed with SAMtools (Li et al., 2009) (v1.9). A custom Python script was used to filter the SAM file for aligned reads with the supplementary alignment (0 × 800) flag, and to filter for reads with overlap of the integration site. Specifically, the start alignment position of the read was used to verify that the read started at least 30bp downstream of the integration site and the cigar string was parsed to verify that the read extended past 30bp upstream of the integration site; the integration site position varied with each gene. For cumulative read counts, the SAM file was then parsed with a custom Python script and each read that contained an indel was tallied. For positional read counts, Picard (http://broadinstitute.github.io/picard) was used to add read group information and index the bam file. Indels were then called with GATK HaplotypeCaller (McKenna et al., 2010) (v3.8-1-0-gf15c1c3ef). In order to call indels on all reads, some parameters were modified from default (min_mapping_quality_score = 0; min_base_quality_score = 0, max_alternate_alleles = 50, output_mode = EMIT_ALL_SITES, emitRefConfidence = BP_RESOLUTION). The resulting VCF file was then filtered to exclude any sites with single nucleotide polymorphisms and to count the number of reads at each site containing an insertion or deletion. For all analyses, each of the three pools were treated independently until calculation of mean and standard error of the mean for both positional and cumulative data.

For quantitative estimation of allelic mutation rate without donor insertion, raw paired-end read sequences of the across-junction PCR products were trimmed of adaptor and poor-quality sequences using Trimmomatic (Bolger et al., 2014) and demultiplexed using Cutadapt (Martin, 2011). The quality of the raw reads was verified by examining the FastQC (v 0.11.8). The paired-end reads were merged with FLASH (Magoč and Salzberg, 2011). The merged reads were then aligned to reference amplicon sequences using EMBOSS Needle (Chojnacki et al., 2017). Finally, the aligned reads were analyzed using CRISPResso for quantification of position and type of mutations within the amplicon sequences (Pinello et al., 2016). Rates of allelic mutations without donor insertion were estimated by the fractions of reads with mutations within the population that lack donor integration. For all analyses, each of the three pools were treated independently until calculation of mean and standard error of the mean.

Neuron, Volume *103*

Supplemental Information

Plug-and-Play Protein Modification Using Homology-Independent Universal Genome Engineering

Yudong Gao, Erin Hisey, Tyler W.A. Bradshaw, Eda Erata, Walter E. Brown, Jamie L. Courtland, Akiyoshi Uezu, Yu Xiang, Yarui Diao, and Scott H. Soderling

Figure S1

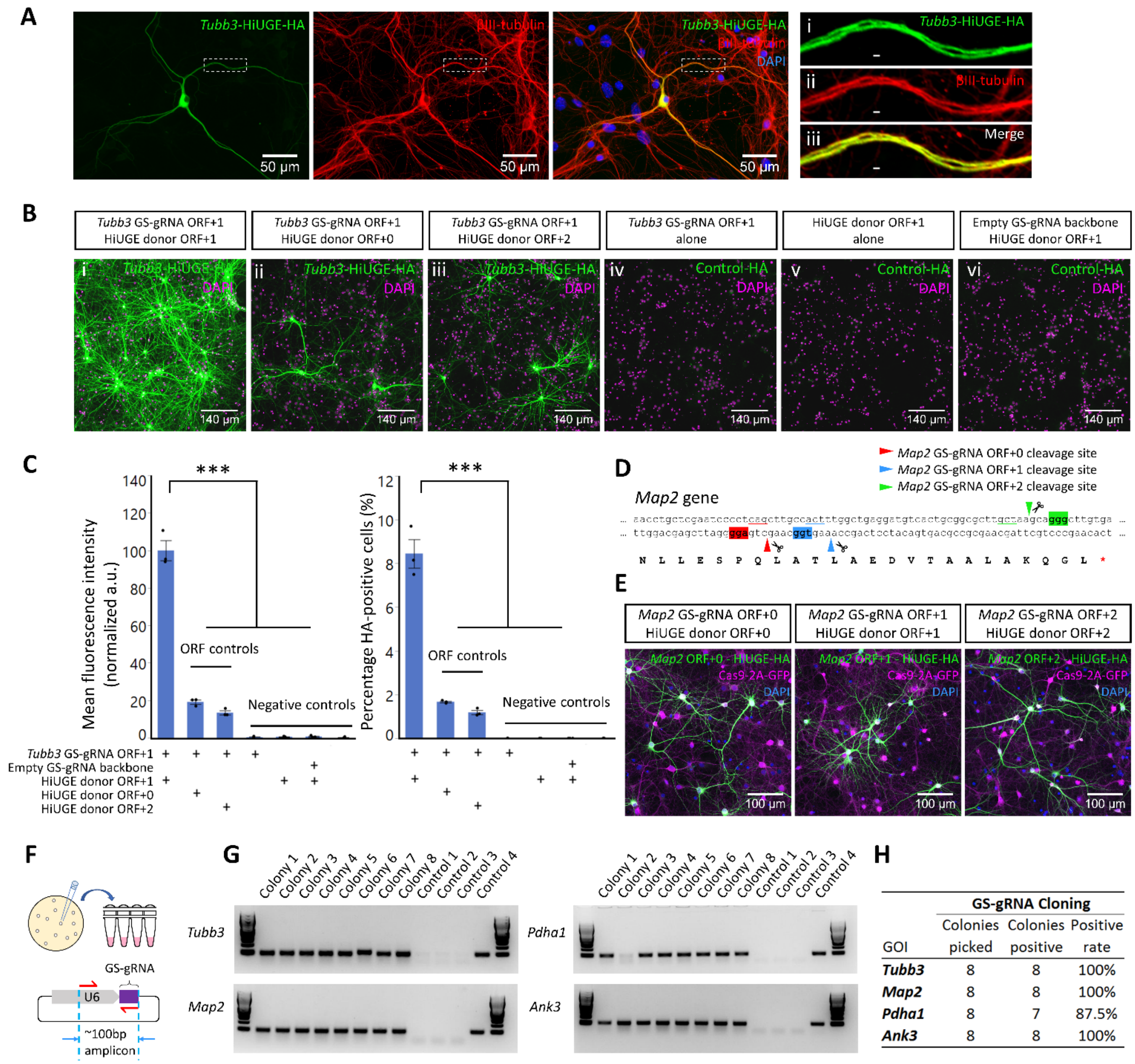
A
Tubb3-HiUGE-HA
βIII-tubulin
Tubb3-HiUGE-HA
βIII-tubulin
DAPI
50 µm
50 µm
50 µm
i
Tubb3-HiUGE-HA
ii
βIII-tubulin
iii
Merge
B
Tubb3 GS-gRNA ORF+1 HiUGE donor ORF+1
Tubb3 GS-gRNA ORF+1 HiUGE donor ORF+0
Tubb3 GS-gRNA ORF+1 HiUGE donor ORF+2
Tubb3 GS-gRNA ORF+1 alone
HiUGE donor ORF+1 alone
Empty GS-gRNA backbone HiUGE donor ORF+1
i Tubb3-HiUGE-HA DAPI
ii Tubb3-HiUGE-HA DAPI
iii Tubb3-HiUGE-HA DAPI
iv Control-HA DAPI
v Control-HA DAPI
vi Control-HA DAPI
140 µm
C
***
Mean fluorescence intensity (normalized a.u.)
0
20
40
60
80
100
120
140
ORF controls
Negative controls
***
Percentage HA-positive cells (%)
0
2
4
6
8
10
12
ORF controls
Negative controls
Tubb3 GS-gRNA ORF+1
Empty GS-gRNA backbone
HiUGE donor ORF+1
HiUGE donor ORF+0
HiUGE donor ORF+2
D
Map2 GS-gRNA ORF+0 cleavage site
Map2 GS-gRNA ORF+1 cleavage site
Map2 GS-gRNA ORF+2 cleavage site
Map2 gene
… aacctgctcgaatcccctcagcttgccactttggctgaggatgtcactgcggcgcttgctaagcagggcttgtga …
… ttggacgagcttaggggagtcgaacggtgaaaccgactcctacagtgacgccgcgaacgattcgtcccgaacact …
N L L E S P Q L A T L A E D V T A A L A K Q G L *
E
Map2 GS-gRNA ORF+0 HiUGE donor ORF+0
Map2 GS-gRNA ORF+1 HiUGE donor ORF+1
Map2 GS-gRNA ORF+2 HiUGE donor ORF+2
Map2 ORF+0 - HiUGE-HA Cas9-2A-GFP DAPI
Map2 ORF+1 - HiUGE-HA Cas9-2A-GFP DAPI
Map2 ORF+2 - HiUGE-HA Cas9-2A-GFP DAPI
100 µm
F
GS-gRNA
U6
~100bp amplicon
G
Colony 1
Colony 2
Colony 3
Colony 4
Colony 5
Colony 6
Colony 7
Colony 8
Control 1
Control 2
Control 3
Control 4
Tubb3
Map2
Pdha1
Ank3
H

	GS-gRNA Cloning		
GOI	Colonies picked	Colonies positive	Positive rate
Tubb3	8	8	100%
Map2	8	8	100%
Pdha1	8	7	87.5%
Ank3	8	8	100%

Figure S1. Additional Qualitative and Quantitative Data of Proof-of-principle Experiments, Related to Figure 1 and Figure 2.

(**A**) Immunolabeling of HiUGE-mediated HA-epitope KI to mouse *Tubb3* (green), counterstained with an anti-βIII-tubulin antibody (red). Colocalization of the fluorescent signal (yellow) is evident. Subpanels (i-iii) show enlarged views of the boxed region from the left. Scale bar is indicated in each panel, or within insets (2µm). (**B**) Representative immunolabeling of HiUGE-mediated HA-epitope KI to *Tubb3* in a control experiment after transduction with equal amount of AAV (5×10^{10} GC / mL per virus in the culture medium), showing HA-epitope immunoreactivity of (i) correct pairing of GS-gRNA and HiUGE donor open reading frame (ORF); (ii-iii) incorrect pairing of GS-gRNA and HiUGE donor ORFs; (iv-vi) negative controls. Nuclei labeling with DAPI and the scale bar are indicated in each panel. (**C**) Quantification of (**B**), showing the normalized mean fluorescence intensities (arbitrary units, a.u.) and the

HA-positive neurons as a percentage of all cells (DAPI positive, including neuronal and non-neuronal cells) across experimental groups. Error bars represent standard error of the mean (SEM). Correct ORF pairing of *Tubb3* GS-gRNA and HiUGE donor showed significantly higher HA-epitope fluorescence intensity over ORF-mismatched controls and negative controls (***: $p < 0.001$, one-way ANOVA followed by Tukey-Kramer HSD *post hoc* test, n=3). Also, HA-labeling in the correct ORF was approximately five fold more efficient (8.4 ± 0.7 % of all cells) compared to occasional HA-positive cells observed from out-of-frame ORFs (ORF+0: 1.7 ± 0.04 %; ORF+2: 1.2 ± 0.1 %. ***: $p < 0.001$, one-way ANOVA followed by Tukey-Kramer HSD *post hoc* test, n=3). Of note, due to the presence of glia cells in the co-culture that do not express the neuronal specific ßIII-tubulin, the cellular labeling efficiency is under-estimated. (**D**) To demonstrate the flexibility of GS-gRNA selection and the capability of HiUGE donor vectors of all three open reading frames (ORFs) to facilitate protein modification, three different GS-gRNAs, one for each ORF (ORF+0, ORF+1, ORF+2), were designed to target mouse *Map2* gene. Shaded DNA triplets denote the protospacer adjacent motif (PAM) of the target sequence for each GS-gRNA. Underlined DNA triplets denote the last codon before the Cas9 cleavage site for each GS-gRNA. (**E**) Representative images showing comparable detection of HA-epitope KI when GS-gRNAs of each ORF were paired with HiUGE donors of the corresponding ORF. GFP fluorescence of the Cas9-2A-GFP, nuclei labeling with DAPI, and the scale bar are indicated in each panel. **(F)** Illustration of colony PCR screening to demonstrate GS-gRNA cloning efficiency. 23-24mer GS-gRNA oligos of four exemplary genes (mouse *Tubb3*, *Map2*, *Pdha1*, and *Ank3*) were annealed and ligated into the SapI sites of GS-gRNA plasmids. Colony PCRs were performed using a common forward primer in the upstream U6 promotor region paired with the reverse GS-gRNA oligo of each gene as the reverse primer to detect a ~100bp amplicon when the GS-gRNAs were successfully integrated. (**G**) Eight colonies (Colony 1-8) were randomly picked from each LB plate and used as PCR template to screen for successful GS-gRNA integration. Control conditions (Control 1-4) include template materials from: (1) non-colony areas on the LB plate, (2) empty GS-gRNA backbone plasmid, (3) water, and (4) positive control with previously sequenced GS-gRNA plasmid for each gene. (**H**) Positive rates of GS-gRNA integration are calculated, showing the cloning method is highly robust and efficient.

Figure S2

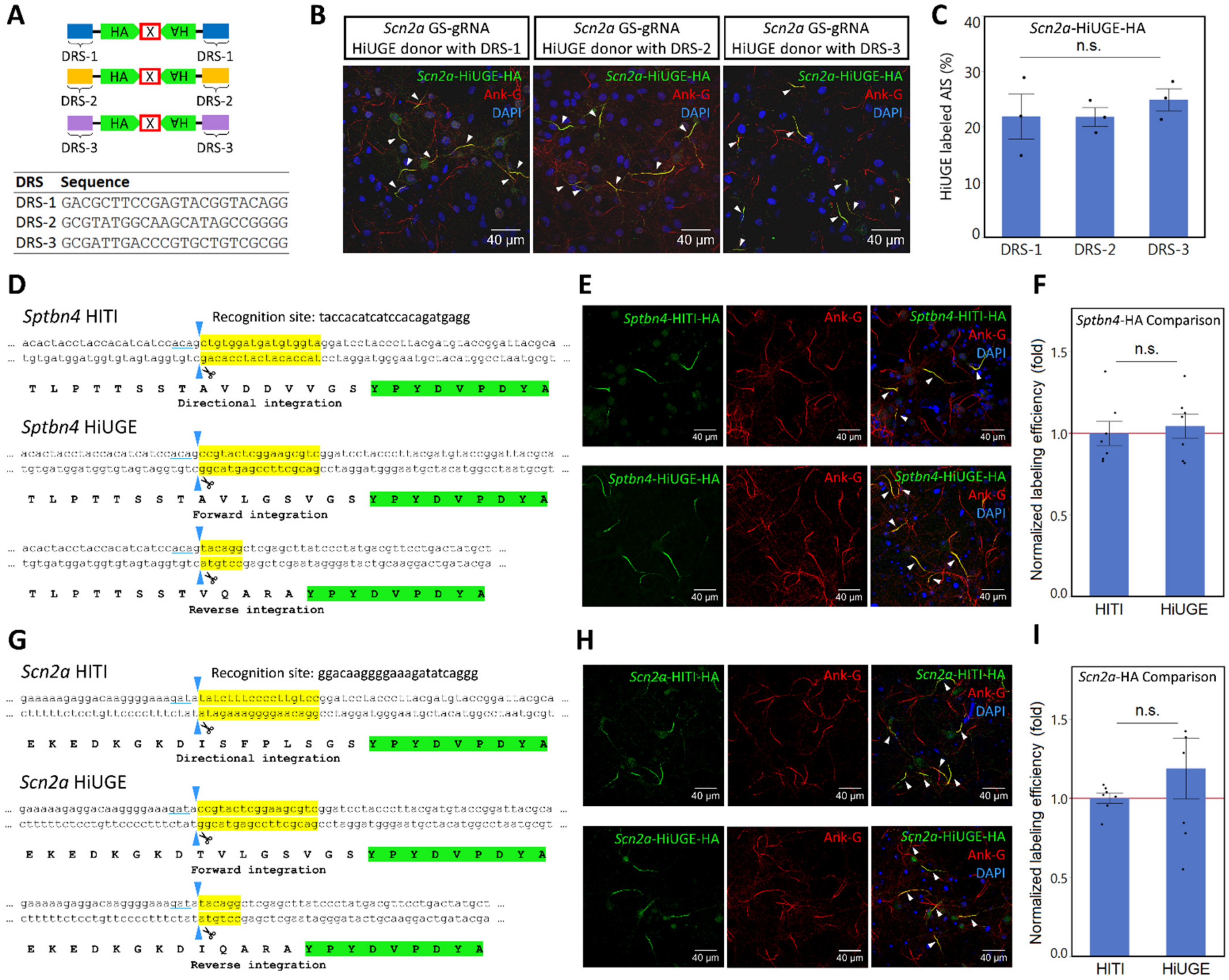

Figure S2. Additional Data of the Comparison Between Different Donor Recognition Sequences and Between HiUGE and HITI, Related to Figure 1 and Figure 2.

(**A**) Three HA-epitope donor vectors containing different HiUGE DRS sequences are compared in an experiment to assess their effectiveness for protein labeling. (**B**) Representative images of HiUGE-mediated HA-epitope labeling of NaV1.2 (encoded by mouse *Scn2a*) using donor vectors with three different DRS sequences (DRS1-3) are shown. Equal amount of virus (5×10^{10} GC / mL per virus in the culture medium) was used. Consistent labeling pattern specific to the axonal initial segment (AIS) is evident. Total AIS structures stained with an AIS-marker (Ank-G) is shown (red), which colocalizes with the HA-labeling (green, arrowheads). (**C**) Quantification result showing similar cellular labeling efficiencies using donor vectors with DRS1-3 (n.s.: $p > 0.05$, one-way ANOVA, n=3). (**D**) Illustration of the genomic sequences following HITI or HiUGE editing of mouse *Sptbn4*. Parts of donor recognition sequences (yellow), inserted HA-epitope peptide (green), and the last coding triplets before the junction (underlined) are highlighted. (**E**) Representative immunofluorescent images showing labeling pattern specific to the AIS following both HITI and HiUGE editing of mouse *Sptbn4*. (**F**) Quantification results showing comparable cellular labeling efficiencies after HITI or HiUGE editing of mouse *Sptbn4* (n.s.: $p > 0.05$, two-tailed t-test, n=7). (**G**) Illustration of the genomic sequences following HITI or HiUGE editing of mouse *Scn2a*. Parts of donor recognition sequences (yellow), inserted HA-epitope peptide (green), and the last coding triplets before the junction (underlined) are highlighted. (**H**) Representative immunofluorescent images showing labeling pattern specific to the AIS following both HITI and HiUGE editing of mouse *Scn2a*. (**I**) Quantification results showing comparable cellular labeling efficiencies after HITI or HiUGE editing of mouse *Scn2a* (n.s.: $p > 0.05$, two-tailed t-test, n=7). Error bars represent standard error of the mean (SEM). Scale bar is indicated in each panel.

Figure S3

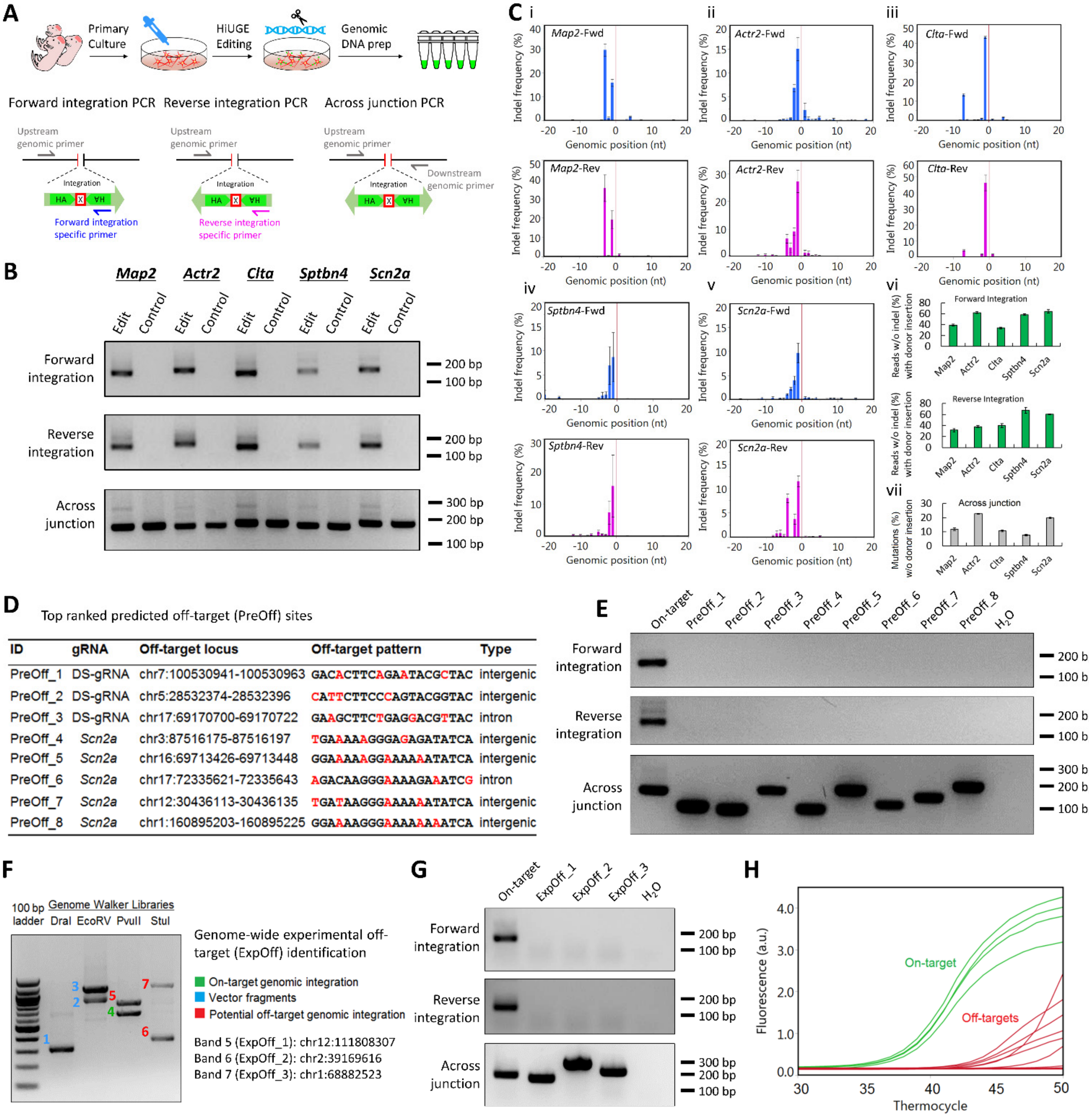

Top ranked predicted off-target (PreOff) sites

ID	gRNA	Off-target locus	Off-target pattern	Type
PreOff_1	DS-gRNA	chr7:100530941-100530963	GACACTTCAGAATACGCTAC	intergenic
PreOff_2	DS-gRNA	chr5:28532374-28532396	CATTCTTCCCAGTACGGTAC	intergenic
PreOff_3	DS-gRNA	chr17:69170700-69170722	GAAGCTTCTGAGGACGTTAC	intron
PreOff_4	*Scn2a*	chr3:87516175-87516197	TGAAAAAGGGAGAGATATCA	intergenic
PreOff_5	*Scn2a*	chr16:69713426-69713448	GGAAAAAGGAAAAAATATCA	intergenic
PreOff_6	*Scn2a*	chr17:72335621-72335643	AGACAAGGGAAAAGAAATCG	intron
PreOff_7	*Scn2a*	chr12:30436113-30436135	TGATAAGGGAAAAAATATCA	intergenic
PreOff_8	*Scn2a*	chr1:160895203-160895225	GGAAAAGGGAAAAAAAATCA	intergenic

Figure S3. Assessment of the Indel Rate and the Off-target Integration of the Donor, Related to Figure 2.

(**A**) Schematic design of genomic PCR to detect dual-orientation HA-epitope payload integration into various genomic loci. Genomic DNAs were extracted from primary neuronal cultures either with or without HiUGE editing. PCR reactions were performed using upstream genomic forward primers of 5 genes (mouse *Map2*, *Actr2*, *Clta*, *Sptbn4*, and *Scn2a*), paired with either a reverse primer specific for the forward payload integration event, or a reverse primer specific for the reverse payload integration event. (**B**) Insert-specific PCRs for both forward and reverse payload integration showed positive bands (~150-

200 bp) in edited samples, compared to no band in negative controls. Across junction PCR of each genomic locus is also shown. Predicted sizes of amplicons (*Map2*, *Actr2*, *Clta*, *Sptbn4*, and *Scn2a*, from left to right respectively) were: forward integration: 168, 193, 156, 168, 174 bp; reverse integration: 157, 182, 145, 157, 163 bp; across junction: 159, 157, 166, 159, 182 bp. (**C**) Analysis of indel frequencies by deep sequencing the PCR products from (**B**). Detections of indel positions (i-v) showed that most indel events initiated immediately adjacent to the edited junction (denoted by 0 on the x-axis, red line). The values on x-axis denote the onset positions of indels called by GATK HaplotypeCaller, with the inserted or deleted sequences immediately succeeding that position. Proportions of reads without an indel from the insert-specific amplicons are also plotted (vi), showing the estimated frequencies of payload integrations without an indel across five genes in both orientations. In addition, the frequencies of allelic mutations without donor integration are estimated at each edited locus by deep sequencing the across junction PCR products (vii). (**D**) Top ranked CRISPOR-predicted off-target loci for both DS-gRNA and *Scn2a* GS-gRNA. (**E**) Genomic PCR reactions using gene-specific primers paired with payload-specific primers successfully detected on-target integrations, while the genomic integrations of the payload were undetected for the predicted off-target sites (PreOff_1-8). Across junction PCR reactions showed robust and specific amplifications using these genomic primers. Predicted sizes of amplicons (On-target and PreOff_1 - 8, from left to right respectively) were: forward integration: 174, 147, 164, 194, 173, 223, 178, 216, 255 bp; reverse integration: 163, 136, 153 ,183, 162, 212, 167, 205, 244 bp; across junction: 182, 117, 105, 188, 110, 199, 131, 165, 227 bp. (**F**) Genome Walker experiment using nested two-round PCR detected on-target integration (band 4), and 3 potential off-target integrations into the non-coding genomic regions (band 5-7). Vector fragments were also detected as expected (band 1-3). (**G**) Genomic PCR reactions using gene-specific primers paired with insert-specific primers successfully detected on-target integrations, while the genomic integrations of the payload were undetected for the experimentally identified potential off-target sites (ExpOff_1-3). Across junction PCR reactions showed robust and specific amplifications using these genomic primers. Predicted sizes of amplicons (On-target and ExpOff_1 - 3, from left to right respectively) were: forward integration: 174, 172, 287, 183 bp; reverse integration: 163, 161, 276, 172 bp; across junction: 182, 158, 309, 220 bp. (**H**) Comparison of real-time PCR amplification curves of on-target integrations (green) versus potential off-target integrations (red). These results are qualitative due to the possible bias of different primers. DNA sizes are marked in reference to the ladder. Genomic positions are in reference to the GRCm38 (mm10) assembly.

Figure S4

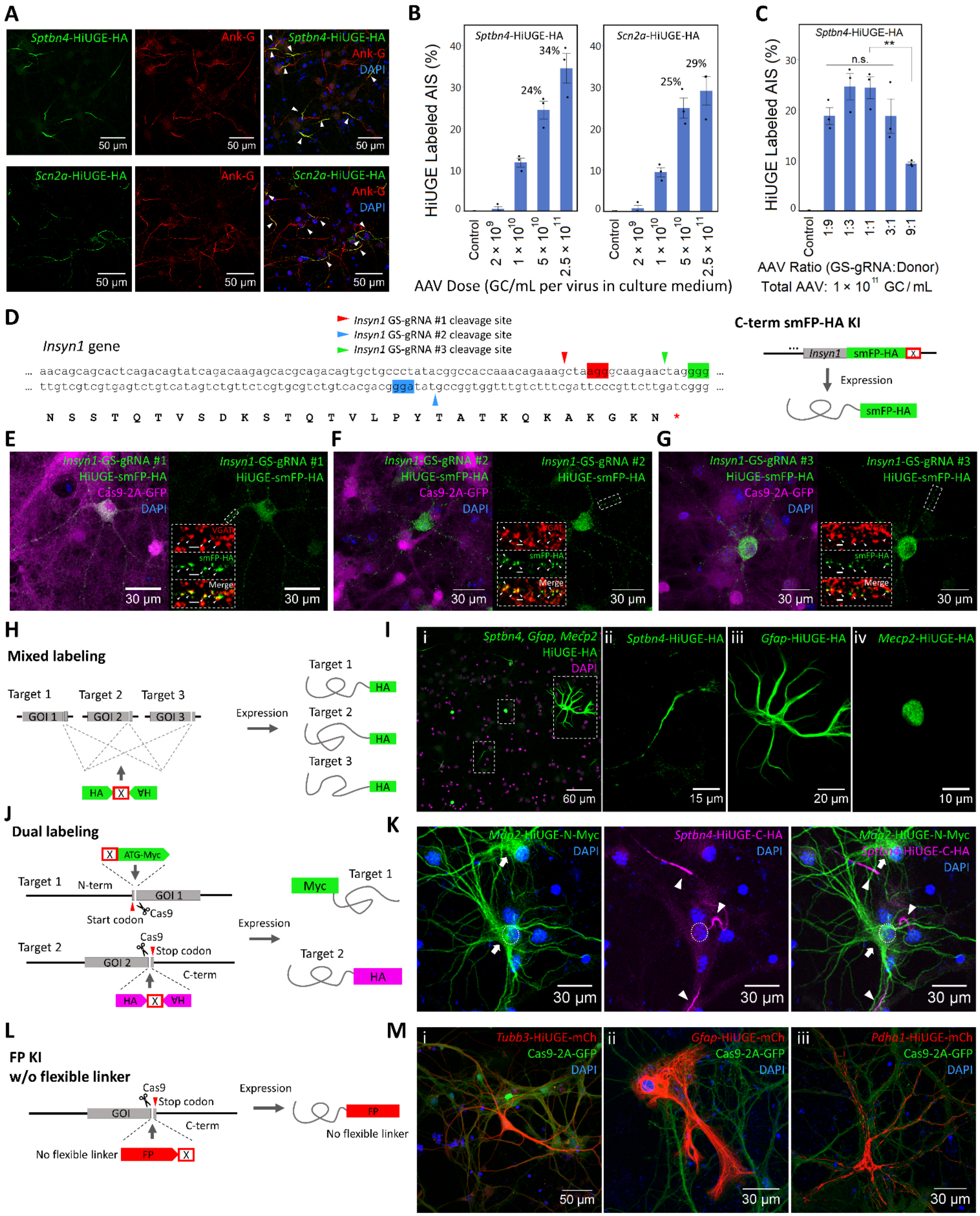

A
Sptbn4-HiUGE-HA
Ank-G
DAPI
Scn2a-HiUGE-HA
50 μm
B
Sptbn4-HiUGE-HA
Scn2a-HiUGE-HA
HiUGE Labeled AIS (%)
0
10
20
30
40
24%
34%
25%
29%
Control
2 × 10^9
1 × 10^10
5 × 10^10
2.5 × 10^11
AAV Dose (GC/mL per virus in culture medium)
C
Sptbn4-HiUGE-HA
n.s.
**
Control
1:9
1:3
1:1
3:1
9:1
AAV Ratio (GS-gRNA:Donor)
Total AAV: 1 × 10^11 GC/mL
D
Insyn1 GS-gRNA #1 cleavage site
Insyn1 GS-gRNA #2 cleavage site
Insyn1 GS-gRNA #3 cleavage site
Insyn1 gene
… aacagcagcactcagacagtatcagacaagagcacgcagacagtgctgccctatacggccaccaaacagaaagctaagggcaagaactagggg …
… ttgtcgtcgtgagtctgtcatagtctgttctcgtgcgtctgtcacgacgggatatgccggtggtttgtctttcgattcccgttcttgatcggg …
N S S T Q T V S D K S T Q T V L P Y T A T K Q K A K G K N *
C-term smFP-HA KI
Insyn1
smFP-HA
X
Expression
smFP-HA
E
F
G
Insyn1-GS-gRNA #1
Insyn1-GS-gRNA #2
Insyn1-GS-gRNA #3
HiUGE-smFP-HA
Cas9-2A-GFP
DAPI
VGAT
smFP-HA
Merge
30 μm
H
Mixed labeling
Target 1
Target 2
Target 3
GOI 1
GOI 2
GOI 3
HA
X
AH
Expression
HA
I
i
Sptbn4, Gfap, Mecp2
HiUGE-HA
DAPI
ii
Sptbn4-HiUGE-HA
iii
Gfap-HiUGE-HA
iv
Mecp2-HiUGE-HA
60 μm
15 μm
20 μm
10 μm
J
Dual labeling
X
ATG-Myc
Target 1
N-term
GOI 1
Cas9
Start codon
Target 2
Cas9
Stop codon
GOI 2
C-term
HA
X
AH
Expression
Myc
Target 1
Target 2
HA
K
Map2-HiUGE-N-Myc
Sptbn4-HiUGE-C-HA
DAPI
30 μm
L
FP KI
w/o flexible linker
Cas9
Stop codon
GOI
C-term
No flexible linker
FP
X
Expression
FP
No flexible linker
M
i
Tubb3-HiUGE-mCh
ii
Gfap-HiUGE-mCh
iii
Pdha1-HiUGE-mCh
Cas9-2A-GFP
DAPI
50 μm
30 μm

Figure S4. Additional Data of the Localization Mapping Application Using HiUGE, Related to Figure 2 and Figure 6.

(**A**) Representative images of HiUGE labeling of AIS proteins βIV-Spectrin and NaV1.2 by C-term HA-epitope KI to mouse *Sptbn4* and *Scn2a*, at high AAV concentrations in primary neuronal culture (2.5 ×

10^{11} GC / mL per virus in culture medium). Immunofluorescent staining with an antibody against AIS-marker Ankyrin-G (Ank-G) is also shown. Arrowheads represent the HiUGE-labeled AIS structures. (**B**) Quantification results showing the estimated efficiencies of cellular labeling across several AAV concentrations at 1:1 virus ratio (GS-gRNA : donor). Efficient labeling was achieved at a dose of 5 × 10^{10} GC / mL per virus (*Sptbn4*: 24.4 ± 2.2 %; *Scn2a:* 24.9 ± 2.4 %), or 2.5 × 10^{11} GC / mL per virus (*Sptbn4*: 34.5 ± 3.6 %; *Scn2a:* 29.0 ± 3.4 %). (**C**) Quantification results showing the estimated efficiencies of cellular labeling across several ratios of AAVs (GS-gRNA : donor) at 1 × 10^{11} GC / mL combined viral concentration in the culture medium. Ratios of 1:9, 1:3, 1:1 and 3:1 were largely equivalent in labeling efficiency (n.s.: $p > 0.05$, one-way ANOVA followed by Tukey-Kramer HSD *post hoc* test, n=3), suggesting a broad range of acceptable viral ratios. However, cellular labeling efficiency of 9:1 ratio is significantly lower compared to 1:1 ratio (**: $p < 0.01$, one-way ANOVA followed by Tukey-Kramer HSD *post hoc* test, n=3), suggesting that sufficient donor AAV is required for efficient labeling. (**D**) Schematic illustration of HiUGE C-term smFP-HA KI to mouse *Insyn1*, directed by three different GS-gRNAs. Shaded DNA triplets denote the protospacer adjacent motif (PAM) of the target sequence for each GS-gRNA. Arrowheads denote the Cas9 cleavage sites. (**E**-**G**) Sucessful and comparable punctate labeling at inhibitory synapses was obsereved across all three GS-gRNAs. Colocalization of the HA-immunoreactivity with the juxtaposed inhibitory presynaptic marker vesicular GABA transporter (VGAT) immunosignal is shown in the insets (arrowheads). (**H**) Various GS-gRNAs targeting different genes can be combined and applied simultaneously with a single HiUGE donor to create mixed labeling. (**I**) Simultaneous labeling of ßIV-spectrin, GFAP, and MeCP2 by pooled application of GS-gRNAs targeting mouse *Sptbn4, Gfap,* and *Mecp2* genes, together with the HA-epitope donor. Panels (ii-iv) are enlarged views of the boxed regions in (i). (**J**) Schematic illustration of HiUGE amino-terminus (N-term) KI construct to achieve dual-labeling of two different targets by differentially targeting the N-term or the C-term of two different proteins. The stop codon cassette within the N-term HiUGE donor vector ensures that in the event of integration into the C-term, the translation will terminate upstream of the Myc-epitope, thus this payload is selective for N-term expression. (**K**) Representative dual-labeled immunostaining image of mouse *Map2* and *Sptbn4* encoded proteins by N-term KI of Myc-epitope to *Map2* (MAP2, arrows), and C-term KI of HA-epitope to *Sptbn4* (ßIV-spectrin, arrowheads). Dashed circle represents the soma of the dual-labeled neuron. (**L**) Fluorescent protein (FP) payloads can be directly fused with endogenous targets (in contrast to being separated by a flexible $(GGGGS)_4$ linker, Figure 6A), enabling flexible selection of linker sequences using HiUGE. (**M**) Representative images of direct mCherry (mCh) fluorescence of HiUGE labeled (i) βIII-tubulin, (ii) GFAP, and (iii) Pyruvate dehydrogenase E1 alpha, using a mCh payload without flexible linker. Scale bar is indicated in each panel, or within insets (2µm).

Figure S5

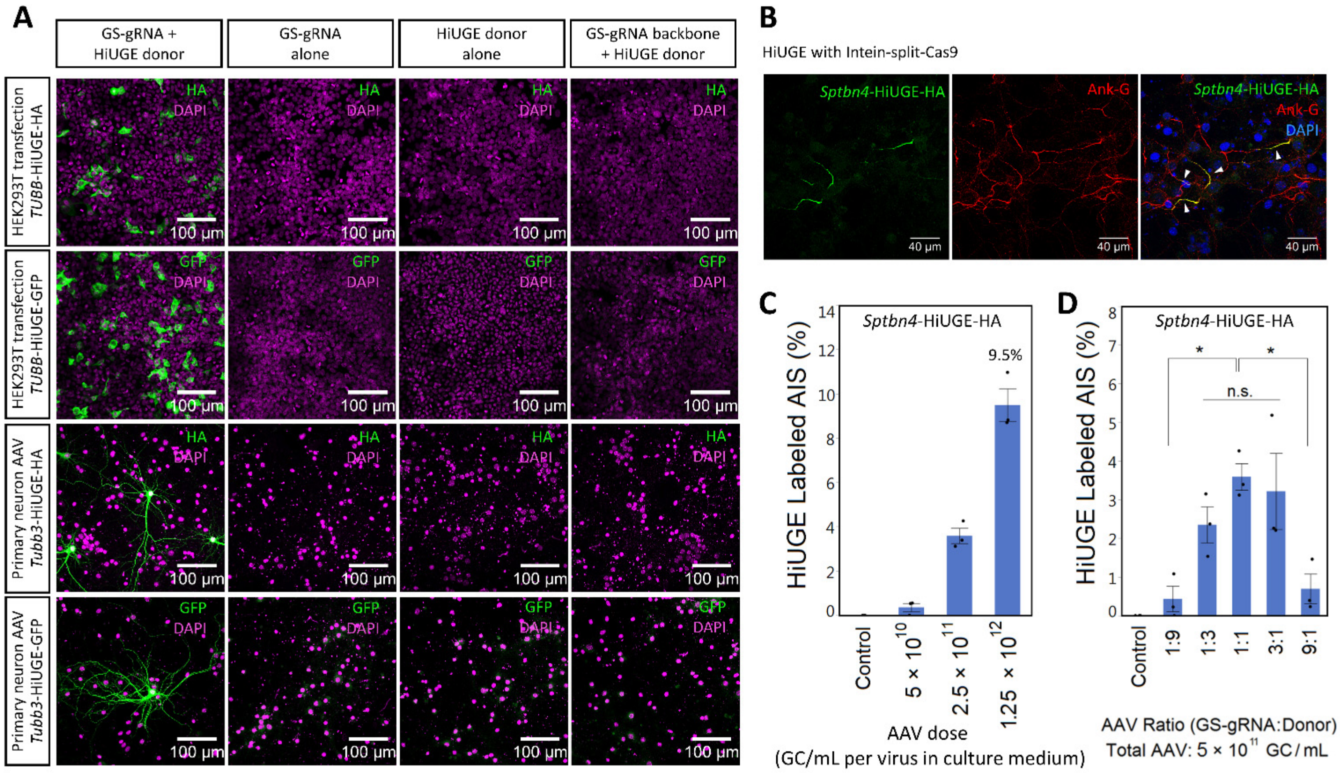
A
GS-gRNA + HiUGE donor
GS-gRNA alone
HiUGE donor alone
GS-gRNA backbone + HiUGE donor
HEK293T transfection TUBB-HiUGE-HA
HEK293T transfection TUBB-HiUGE-GFP
Primary neuron AAV Tubb3-HiUGE-HA
Primary neuron AAV Tubb3-HiUGE-GFP
HA
GFP
DAPI
100 µm
B
HiUGE with Intein-split-Cas9
Sptbn4-HiUGE-HA
Ank-G
DAPI
40 µm
C
Sptbn4-HiUGE-HA
9.5%
HiUGE Labeled AIS (%)
0
2
4
6
8
10
12
14
Control
5 × 10^10
2.5 × 10^11
1.25 × 10^12
AAV dose
(GC/mL per virus in culture medium)
D
Sptbn4-HiUGE-HA
HiUGE Labeled AIS (%)
0
1
2
3
4
5
6
7
8
*
*
n.s.
Control
1:9
1:3
1:1
3:1
9:1
AAV Ratio (GS-gRNA:Donor)
Total AAV: 5 × 10^11 GC / mL

Figure S5. Additional Data of HiUGE Vectors with Intein-Split-Cas9, Related to Figure 7.

(**A**) Control experiments for intein-split-Cas9 mediated HiUGE vectors in HEK293T cells and WT primary neurons. HEK293T Cells were plasmid transfected and primary neurons were AAV transduced with HiUGE GS-gRNAs and donors to knock-in HA-epitope or GFP payloads to human *TUBB* or mouse *Tubb3* genomic loci. Experimental conditions are indicated in the figure. Positive HA-epitope or GFP immunoreactivity showing tubulin-like expression pattern was only found when GS-gRNAs were paired with the corresponding HiUGE donors (*leftmost column*). No HA-epitope or GFP KI was detected when GS-gRNA or HiUGE donor was applied alone, or when an empty GS-gRNA backbone was paired with the donor. (**B**) Representative images showing labeling of βIV-spectrin (*Sptbn4*) using HiUGE with intein-split-Cas9 at the viral dose of 1.25×10^{12} GC / mL per virus in the culture medium. Arrowheads represent the HiUGE-labeled AIS structures. (**C**) Quantification results showing the estimated efficiencies of cellular labeling across several AAV concentrations at a 1:1 virus ratio (GS-gRNA : donor). Labeling efficiency of 9.5 ± 0.7 % was achieved at the dose of 1.25×10^{12} GC / mL per virus in culture medium. (**D**) Quantification results showing the estimated efficiencies of cellular labeling across several ratios of AAVs (GS-gRNA : donor) at 5×10^{11} GC / mL combined viral concentration in the culture medium. At ratios of 1:3, 1:1 and 3:1 there were no significant differences in labeling efficiency (n.s.: $p > 0.05$, one-way ANOVA followed by Tukey-Kramer HSD *post hoc* test, n=3). However, cellular labeling efficiencies at 1:9 or 9:1 ratio were significantly lower compared to the 1:1 ratio (*: $p < 0.05$, one-way ANOVA followed by Tukey-Kramer HSD *post hoc* test, n=3). Error bars represent standard error of the mean (SEM). Scale bar is indicated in each panel.